

NLR TP 93288 U

# NATIONAAL LUCHT- EN RUIMTEVAARTLABORATORIUM

NATIONAL AEROSPACE LABORATORY NLR

THE NETHERLANDS

Bibliotheek TU Delft  
Faculteit der Luchtvaart- en Ruimtevaarttechniek  
Kluyverweg 1  
2629 HS Delft

NLR TP 93288 U

29 AUG. 1994

EFFECT OF COOLING RATE ON INTERLAMINAR FRACTURE ENERGY  
AND SHEAR STRENGTH OF APC-2 LAMINATES

by

W. van der Hoeven



Reprints from this document may be made on condition that full credit is given to the Nationaal Lucht- en Ruimtevaartlaboratorium (National Aerospace Laboratory NLR) and the author(s).

**NATIONAAL LUCHT- EN RUIMTEVAARTLABORATORIUM**  
NATIONAL AEROSPACE LABORATORY NLR



---

Anthony Fokkerweg 2, 1059 CM AMSTERDAM, The Netherlands  
P.O. Box 90502 , 1006 BM AMSTERDAM, The Netherlands  
Telephone : 31-(0)20-5 11 31 13  
Fax : 31-(0)20-5 11 32 10

2102956

DOCUMENT CONTROL SHEET

	ORIGINATOR'S REF. NLR TP 93288 U		SECURITY CLASS. Unclassified
ORIGINATOR National Aerospace Laboratory NLR, Amsterdam, The Netherlands			
TITLE Effect of cooling rate on interlaminar fracture energy and shear strength of APC-2 laminates.			
PRESENTED AT			
AUTHORS W. van der Hoeven		DATE 930531	pp ref 63 16
DESCRIPTORS (NASA Language) Carbon fibre reinforced plastics      Polymer matrix composites Peek      Laminates Thermoplastic resins      Crack opening displacement Fracture strength      Cooling Temperature effects      Auto claving Strain energy release rate			
ABSTRACT The effect of cooling rate on some mechanical properties of APC-2/AS4 composite was investigated over the range between 1 and 70° C/min. Preconsolidated unidirectional laminates were reprocessed in a hot platen press at controlled cooling rates. <u>Double Cantilever Beam</u> specimens and <u>End Notch Flexure</u> specimens were used to determine the mode I and mode II fracture energies, respectively. The interlaminar shear properties were measured using the Iosupescu shear test method. The results indicated that the shear modulus and the shear strenght tended to decrease slightly with increasing cooling rate. The mode I fracture energy was observed to increase with cooling rate by about 8 per cent within the range investigated. The type of precrack was found to have a significant effect on the mode II fracture energy calculated from the test results. Specimens with mechanically induced precracks yielded fracture energies that were significantly lower than those for specimens with moulded-in precracks. For specimens with mechanically induced precracks the mode II fracture energy was found to increase with cooling rate by about 19 per cent within the range investigated. It is concluded that decreasing the cooling rate below the minimum value specified by the material supplier (10° C/min) will most probably not lead to an abrupt or substantial degradation of the mechanical performance of APC-2.			

Bibliotheek TU Delft/LR



C 2102957

NLR TECHNICAL PUBLICATION

TP 93288 U


EFFECT OF COOLING RATE ON INTERLAMINAR FRACTURE ENERGY  
AND SHEAR STRENGTH OF APC-2 LAMINATES


by

W. van der Hoeven

This investigation has been carried out under a contract awarded by the Netherlands Agency for Aerospace Programs, contract number 01907N.

Division: Structures and Materials

Prepared: WvdH/ 

Approved: RJHW/ 

Completed : 930531

Order number: 101.913

Typ. : MM



#### SUMMARY

The effect of cooling rate on some mechanical properties of APC-2/AS4 composite was investigated over the range between 1 and 70 °C/min. Pre-consolidated unidirectional laminates were reprocessed in a hot platen press at controlled cooling rates. Double Cantilever Beam specimens and End Notch Flexure specimens were used to determine the mode I and mode II fracture energies, respectively. The interlaminar shear properties were measured using the Iosupescu shear test method.

The results indicated that the shear modulus and the shear strength tended to decrease slightly with increasing cooling rate. The mode I fracture energy was observed to increase with cooling rate by about 8 per cent within the range investigated. The type of precrack was found to have a significant effect on the mode II fracture energy calculated from the test results. Specimens with mechanically induced precracks yielded fracture energies that were significantly lower than those for specimens with moulded-in precracks. For specimens with mechanically induced precracks the mode II fracture energy was found to increase with cooling rate by about 19 per cent within the range investigated.

It is concluded that decreasing the cooling rate below the minimum value specified by the material supplier (10 °C/min) will most probably not lead to an abrupt or substantial degradation of the mechanical performance of APC-2.



---

TABLE OF CONTENTS

	Page
<u>1</u> INTRODUCTION	7
<u>2</u> PRODUCTION OF APC-2 SHEETS	8
<u>2.1</u> Autoclave moulding	8
<u>2.2</u> Press moulding	9
<u>2.2.1</u> Cooling curves	10
<u>3</u> MANUFACTURING OF SPECIMENS	11
<u>4</u> TESTING PROCEDURES	12
<u>4.1</u> Mode I fracture energy	12
<u>4.2</u> Mode II fracture energy	13
<u>4.3</u> Iosupescu shear tests	14
<u>4.4</u> Fibre volume content	15
<u>5</u> DATA ANALYSIS	16
<u>5.1</u> Mode I fracture energy	16
<u>5.2</u> Mode II fracture energy	17
<u>5.3</u> Iosupescu shear tests	18
<u>6</u> RESULTS	19
<u>6.1</u> Mode I fracture energy	19
<u>6.2</u> Mode II fracture energy	21
<u>6.3</u> Iosupescu shear tests	24
<u>6.4</u> Fibre volume content	24
<u>7</u> DISCUSSION	25
<u>7.1</u> The effect of cooling rate	25
<u>7.2</u> Evaluation of the test methods	26
<u>8</u> CONCLUSIONS	31



TABLE OF CONTENTS (continued)

	Page
2 REFERENCES	32

9 Tables  
28 Figures

(63 pages in total)



This page is intentionally left blank.





## 1 INTRODUCTION

The development and evaluation of thermoplastic resins as matrices for fibre reinforced composites has received considerable attention in recent years. It has been recognized by the aircraft industries that high performance thermoplastic polymers offer several potential advantages over thermoset polymers. One of the main advantages is their markedly superior damage resistance. Other potential advantages are that the shorter processing times and the unlimited shelf life may reduce the manufacturing costs, and the ability to reprocess the material may contribute to an improved reparability.

APC-2 is generally regarded as one of the most promising thermoplastic composites. It consists of uniaxially aligned carbon fibres embedded in a PEEK (Poly-Ether-Ether-Ketone) matrix. PEEK is a ductile, semicrystalline polymer, and as such the degree of crystallinity and the crystalline morphology will depend on the thermal history and processing conditions, which in turn may affect the mechanical properties of the polymer.

During processing the material is heated to above the melting temperature of the polymer, and subsequently shaped into the desired product form. Upon cooling the polymer it crystallizes. When no additional heat treatment is applied the crystallization process is largely governed by the rate of cooling. According to the material supplier the cooling rate should be in the range between 10 and 700 °C/min in order to achieve the desired properties.

For the production of large structural parts autoclave moulding is probably the most suitable processing route. However, in most autoclaves cooling rates below 10 °C/min cannot be applied. It is therefore to be expected that in future composite parts will have to be produced with cooling rates outside the recommended range. For this reason the NLR started an investigation with the objective of assessing the effect of cooling rate upon the behaviour of APC-2 within the range of low cooling rates (1 to 70 °C/min).

During the first phase of this programme the effect of cooling rate on the crystallinity was investigated using Differential Scanning Calorimetry (Ref. 1). The present report deals with the second phase, in which the effect of cooling rate on some mechanical properties was determined.



In section 2 the procedure used for producing APC-2 sheets is described. Details on the manufacture of test specimens are given in section 3. During this investigation three types of mechanical tests were conducted: mode I and mode II interlaminar fracture energy tests and Iosupescu shear tests. In addition, for each APC-2 sheet the fibre volume fraction was determined. The testing procedures are described in section 4. The results of the tests were analysed by more or less standard analysis procedures, which are described in section 5. The results of the mechanical tests and the fibre volume fraction determination are detailed in section 6 and discussed in section 7. The conclusions are summarized in section 8.

Originally it was also intended to determine the effect of cooling rate on the environmental resistance of APC-2. However, during the present programme the prospects with respect to future availability of the material became uncertain. In consultation with the sponser it was therefore decided to stop the experimental programme after completion of the mechanical tests.

## 2 PRODUCTION OF APC-2 SHEETS

In this section the manufacturing procedure for the APC-2 sheets is described. All sheets were produced using unidirectional APC-2/AS4 prepreg tape supplied by Imperial Chemical Industries (ICI). A two-stage manufacturing process was employed. Firstly, several laminates were consolidated in an autoclave. The consolidated sheets were then reprocessed in a hot platen press and cooled at different rates. The conditions for each of these processes are detailed in the next two sub-sections.

### 2.1 Autoclave moulding

Unidirectional laminates were produced with a nominal thickness of 3 mm (dimensions 540 x 300 mm). Each laminate consisted of 24 prepreg plies. During lay-up the plies were assembled into prepreg stacks of 8 plies. Each ply was bonded to the one below by a series of seam welds made with a soldering iron. At one edge of the laminate a 10  $\mu$ m thick Kapton foil was placed between the second and third prepreg stack. This Kapton foil



would later serve as a precrack in the Double Cantilever Beam (DCB) and End Notch Fracture (ENF) specimens which were to be produced from the sheets.

The laminate was placed on an autoclave table between 1.5 mm thick stainless steel caul plates, and surrounded by a steel picture-frame mould to prevent excessive resin flow near the edges during processing. The gap between the picture-frame and the laminate edges was about 3 mm. The picture frame and caul plates were both coated with release agent. A ventilation blanket was placed on top of the upper caul plate. A vacuum bag was formed by draping a Upilex foil over the lay-up. The foil was airtight clamped to the autoclave table by means of a clamping frame and high temperature sealant tape.

The sheets were consolidated in an air pressurised autoclave using the temperature/pressure cycle shown in figure 1. The maximum cooling rate for the autoclave was about 15 °C/min. In order to increase the cooling rate three consecutive pressure cycles from 0.5 to 0.7 MPa were applied at the start of the cooling step. Each pressure cycle resulted in a partial replacement of the hot air in the autoclave by cold air. After preconsolidation the sheets were ultrasonically C-canned. No defects were observed.

## 2.2 Press moulding

Sheets with dimensions of 297 x 397 mm were machined from the autoclave moulded laminates. These sheets were reprocessed in a computer controlled hot platen press at the Faculty of Aerospace Engineering, Delft University of Technology. Pressing was between mirror finish stainless steel plates using a picture-frame mould with inner dimensions of 300 x 400 mm. During press moulding the temperature of the laminates was recorded using a thermocouple positioned at the laminate midplane at a distance of about 20 mm from the one of the edges.

The applied temperature/pressure cycle is shown in figure 2. The material was heated to 390 °C at a heating rate of about 9 °C/min. During heat up the pressure was 0.5 MPa. This was increased to 1.4 MPa at the onset of the dwell at 390 °C. Figure 2 also shows the temperature response for one of the laminates. As can be seen, the laminate temperature lagged significantly



behind the programmed temperature. Cooling was manually initiated as soon as the material reached a temperature of 380 °C. At the onset of cooling the pressure was further increased to 2 MPa.

Five laminates were produced according to this procedure. These five laminates were programmed to cool at constant cooling rates of 1, 5, 10, 30 and 70 °C/min. The actual cooling rates are reported in the next sub-section. After processing the laminates were ultrasonically C-scanned. The 6 dB attenuation method was used for interpreting the C-scan results, i.e. areas for which the received signal was larger than 50 percent of the transmitted signal were considered to be free of defects. Defects were found in the laminates cooled at 10 and 30 °C/min.

#### 2.2.1 Cooling curves

Cooling curves for the press moulded laminates measured with the thermocouple inside the laminates are shown in figures 3 and 4.

For the laminate programmed to cool at a rate of 70 °C/min the actual cooling rate was about 72 °C/min over the range between 380 and 275 °C. Between 275 and 260 °C the cooling rate first decreased and then increased again, as can be seen in figure 4. This behaviour is most probably due to heat evolved within the material during crystallization.

The temperature fluctuations in the cooling curves for cooling rates lower than 70 °C/min are most probably due to the cooling system of the press, which operated with an on/off water supply to the internally cooled platens.

The crystallization behaviour of the PEEK matrix is largely determined by the cooling rate between the melting temperature and the crystallization temperature. The crystallization temperature itself is a function of the cooling rate, as shown in figure 5. For cooling rates below 70 °C/min the crystallization temperature is higher than 275 °C. For that reason the average cooling rate between 275 °C and 380 °C was taken as the characteristic cooling rate for the APC-2 laminates. These cooling rates are given in the table below.



Programmed cooling rate (°C/min)	Actual average cooling rate above 275 °C (°C/min)
1	1
5	3.7
10	6.5
30	24
70	72

### 3 MANUFACTURING OF SPECIMENS

The specimen types and the number of specimens that were machined from the APC-2 sheets are indicated in the table below. This table also shows the code numbers of the specimens (digit i is used to indicate the programmed cooling rate).

Specimen type	Specimen code	Property to be determined	Number of specimens	Dimensions in cut-up schemes (mm)
Double Cantilever Beam	iA1 to iA3	Mode I fracture energy	3	22 x 265
End Notch Flexure	iB1 to iB5	Mode II fracture energy	5	22 x 112
Iosupescu shear	iC1 to iC5	Shear modulus and strength	5	21 x 78
Environmental resistance	iD1 to iD15	Solvent resistance	15	12 x 46
Fibre volume content	iE1 to iE5	Fibre volume content	5	6 x 62

Examples of cut-up schemes, according to which specimens were sawn from the sheets, are shown in figures 6 and 7. The laminate programmed to cool at a rate of 10 °C/min was the only laminate for which it was not possible to produce all specimens from defect free areas. As can be seen in figure 6, the mode II fracture energy specimens 10B1 to 10B5 were taken from poor quality areas.



#### 4 TESTING PROCEDURES

In this section the applied procedures for the fracture energy tests (mode I and mode II), the Iosupescu shear tests and the fibre volume fraction determinations are described. The data analysis procedures are detailed in section 5.

##### 4.1 Mode I fracture energy

Three Double Cantilever Beam specimens were machined from each APC-2 sheet. The specimen geometry is shown in figure 8. A Kapton film at the laminate mid-thickness, and about 50 mm in length, served as starter notch. For load introduction aluminium blocks containing clevis pin holes were bonded to the specimens using a room temperature curing adhesive (Agomet F310).

All tests were done in a 5 kN Instron screw driven tensile testing machine under displacement control. The clamping arrangement included a universal joint in the load path between the specimen and the upper crosshead of the test machine. During the tests the crack opening displacement (COD) at the load line was measured with two Linear Variable Differential Transformers (LVDT's), one on each side of the specimen, see figure 9. The COD was recorded versus the applied load on an x-y-y recorder. When crack growth was stable the crack was allowed to grow for about 10 mm before the machine was stopped. The crack length was measured before the specimen was unloaded. At the new crack length the procedure was repeated until the total crack length in the specimen was about 150 mm. The crack length was measured on both sides of the specimen using a low power microscope. The positions of the crack tips were marked on the specimen edges. For crack lengths smaller than 60 mm the specimens were loaded at a crosshead speed of 2 mm/min. For crack lengths between 60 and 110 mm the crosshead speed was increased to 5 mm/min and for larger crack lengths the speed was further increased to 10 mm/min. The increase in crosshead speed not only reduced testing time, but also prevented large differences in strain rate at the crack tip for tests with widely different crack lengths (several publications indicate that the mechanical properties of PEEK polymer are strain rate dependent (Refs. 2 and 3)).



#### 4.2 Mode II fracture energy

Five End Notch Flexure (ENF) specimens were produced from each APC-2 sheet. The dimensions of the specimens are also given in figure 8. The length of the specimens was 110 mm, except for specimens 1B1 to 1B5 which were erroneously machined to a length of 100 mm.

The Kapton foil insert at the mid-thickness served as an artificial precrack of about 20 mm in length. A previous investigation had shown that fracture energy values measured with ENF specimens with moulded-in precracks could be significantly higher than those measured with specimens with mechanically induced precracks. In order to create sharp crack tips in the present ENF specimens, the delamination lengths were slightly increased before testing by carefully driving a wedge between the central plies. During this mechanical precracking the specimens were clamped into a bench-vice to prevent excessive crack extension. It was intended to enlarge the delamination to about 35 mm measured from the edge of the specimens, which would require a mechanical extension of about 15 mm for most specimens. However, due to a misunderstanding the actual mechanical crack extensions were generally limited to a few millimetres only.

All tests were done in a 5 kN tensile testing machine with the standard 3-point bending fixture shown in figure 10. The radius of curvature of both outer support pins and that of the central loading pin was 5 mm. The distance between the outer support pins ( $2L$ ) was 80 mm. The specimens were positioned in the fixture such that the crack tip was approximately midway between the central loading pin and one of the outer support pins, i.e.  $a = 20$  mm and  $a/L = 0.5$ . The crack length  $a$  is defined as the distance between the crack tip and the centre line of the nearest outer support pin. Note that due to the small crack lengths the specimens were not symmetrically located in the fixture. The distance  $z$  between the edge of the specimen and the outer support pin was measured before testing, see figure 10. The specimens were loaded at a crosshead speed of 1 mm/min. During the tests the displacement of the central loading point was measured with an LVDT and plotted versus the applied load.



In addition to the five ENF specimens with moulded-in precracks for each cooling rate, two more ENF specimens were made from the remnants of the DCB specimens. This was done by shortening the length of the DCB specimen after mode I testing, such that the distance between the edge of the specimen and the tip of the crack was about 35 mm. These specimens were tested according to the same procedure as described above and will be designated as ENF(DCB) specimens.

#### 4.3 Iosupescu shear tests

The Iosupescu shear test method was originally developed for measurement of the shear properties of metals (Ref. 4). In the late 1970's the method was further developed at the University of Wyoming (Refs. 5 and 6) and applied in studying the shear behaviour of composite materials.

Five Iosupescu shear test specimens were machined from each APC-2 sheet. The dimensions of the specimen are given in figure 11. The specimens were tested with the fixture shown in figure 12. The fibre direction was parallel to the loading axis.

The test fixture consists of two almost identical halves. One half is mounted on the base plate. The other half is movable in the vertical direction along a guide rod. The specimen is clamped into the fixture using wedge clamps, which fully prevent rotation of the specimen ends during loading. During testing an external load is applied directly on top of the movable fixture half. It is assumed that the external load on the fixture results in a state of pure shear in the test section of the specimen ( $x = 0$ ). The V-shaped notches at the midlength of the specimen alter the parabolic shear stress distribution present in constant cross section beams to a uniform stress distribution in the section between the notches. The stress distribution in the specimen was extensively analysed by the authors of references 5 and 6 using a finite element method.

For each series of five shear specimens, four were instrumented with strain gauge rosettes (type HBM 1,5/1200XY21) in the test section. These rosettes were oriented at  $\pm 45$  degrees to the longitudinal axis of the specimen, as shown in figure 11. During the tests the fixture was positioned on a flat





compression platen of a 5 kN Instron tensile test machine. The following specimen installation procedure was used:

The specimen was inserted in the fixture with the strain gauges facing the back side. The specimen was centred in the length (x) direction using a lift alignment tool to index the lower specimen notch. Metal shims between the specimen and the fixture were used to ensure that the loading line coincided with the midplane of the specimen in the width (z) direction. After positioning, the specimen was secured in the fixture by tightening the wedge adjustment screws. The load was introduced through a loading pin fixed to the upper crosshead of the test machine. The deflection of the upper crosshead was measured with an LVDT. All tests were done under displacement control with a crosshead speed of 0.2 mm per minute.

During testing the strains of the tension and compression gauges and the displacement of the upper crosshead were recorded versus the applied load. The notch root areas were viewed with low power magnifying glasses during the final stage of the test.

#### 4.4 Fibre volume content

The fibre volume fraction was determined for each laminate, by acid digestion largely in accordance with a Fokker standard procedure (TH 14.5194). In this procedure the polymer in a laminate sample of known weight and volume is completely oxidized in a moderately heated  $H_2O_2/H_2SO_4$  solution. The carbon fibres are then washed from the solution using a glass filter, which is subsequently dried for 15 minutes at 300 °C. The carbon fibre weight fraction was calculated from the sample weight difference before and after resin digestion.

Five measurements were performed on samples from each laminate. These samples had dimensions of 40 x 6 mm, and a thickness equal to that of the laminate.



## 5 DATA ANALYSIS

In this section the data analysis procedures for the mechanical tests are described.

### 5.1 Mode I fracture energy

The mode I critical energy release rate for initiation of delamination growth was calculated by the well known formula:

$$G_{Ic} = \frac{P_c^2}{2W} \frac{dC}{da} \quad (1)$$

in which:

- $G_{Ic}$  - mode I critical energy release rate
- $P_c$  - maximum load during a test at crack length  $a$
- $a$  - crack length
- $C$  - compliance at crack length  $a$
- $W$  - width of the specimen

In the following,  $G_{Ic}$  will be referred to as the mode I fracture energy. The crack length,  $a$ , was taken as the average of the crack lengths measured on both sides of the specimen. The compliances  $C_1$  and  $C_2$  were determined from the slope of each of the two load-COD records. The average of  $C_1$  and  $C_2$  was used in the calculations.

In order to calculate the fracture energy the compliance-crack length relation has to be known. According to classical beam theory this relation can be approximated by:

$$C = \frac{2a^3}{3EI} \quad (2)$$

in which  $EI$  is the bending stiffness of the cantilever beams. In analyzing the present results a slightly modified expression was used, as suggested in reference 7:

$$C = \frac{2a^3}{3E_{at}I} \quad (3)$$

This modified expression differs from equation 2 in that the bending stiffness of the material is considered to be a function of crack length:



$$E_{af} = E_o \left[ 1 - \frac{a_o}{a} \right] \quad (4)$$

in which  $E_o$  and  $a_o$  are constants, which were calculated for each specimen by the method of least squares using the relations:

$$nE_o = a_o \sum_{i=1}^n \frac{1}{a_i} - \sum_{i=1}^n E_{af_i} = 0 \quad (5)$$

$$E_o \sum_{i=1}^n \frac{1}{a_i} - E_o a_o \sum_{i=1}^n \frac{1}{a_i^2} - \sum_{i=1}^n \frac{E_{af_i}}{a_i} = 0 \quad (6)$$

with

$$E_{af_i} = \frac{8a_i^3}{C_i B t^3} \quad (7)$$

where  $n$  = the number of crack growth tests on a particular specimen, and  
and  $t$  = thickness of a cantilever beam (= half specimen thickness).

The mode I fracture energy was finally calculated from:

$$G_{Ic} = \frac{4P_{c_i}^2 a_i^3}{E_o W^2 t^3} \frac{3a_i - 4a_o}{(a_i - a_o)^2} \quad (8)$$

## 5.2 Mode II fracture energy

The general expression for the mode II critical energy release rate for delamination growth is the same as that for mode I:

$$G_{IIc} = \frac{P^2}{2W} \frac{dC}{da} \quad (9)$$

$G_{IIc}$  will be referred to as the mode II fracture energy. An expression for the compliance,  $C$ , for an ENF specimen can easily be derived using engineering beam theory (Ref. 8):

$$C = \frac{2L^3 + 3a^3}{8EW H^3} \quad (10)$$

where, in addition to the parameters already defined with Eq. 1,  
 $2L$  = total span length (distance between outer supports)



E = Young's modulus of the laminate (in fibre direction).

Substitution of the derivative of the compliance C with respect to crack length (dC/da) in Eq. 9, and subsequent elimination of Young's modulus from the resulting expression results in:

$$G_{IIc} = \frac{9 P_c^2 a^2 C}{2W (2L^3 + 3a^3)} \quad (11)$$

This equation was used in calculating the mode II fracture energy from the present test results.

### 5.3 Iosupescu shear tests

From the recorded load-strain curves the following properties were determined:

1. Shear strength :  $\tau_f$
2. Shear modulus : G
3. Shear strain to failure:  $\gamma_f$

The shear strength was calculated from:

$$\tau = \frac{P_{max}}{W t} \quad (12)$$

in which,  $P_{max}$  = maximum load reached during the test  
B = distance between the notch roots  
t = thickness.

For most specimens the load-strain records were slightly non-linear even at low load levels. The shear modulus was defined as:

$$G = \frac{1}{W t} \frac{\Delta P}{\Delta \gamma} \quad (13)$$

in which  $\Delta\gamma$  is the increase in shear strain when the load is increased from 400 N to 1200 N ( $\Delta P = 800$  N).



For both strain gauges the strain to failure ( $\epsilon^{+45_f}$  and  $\epsilon^{-45_f}$ ) was determined from the recorded load-strain traces. The total shear strain to failure was calculated from:

$$\gamma_f = |\epsilon^{+45_f}| + |\epsilon^{-45_f}| \quad (14)$$

## 6 RESULTS

### 6.1 Mode I fracture energy

#### Load-deflection curves

Typical loading and unloading curves measured during mode I fracture energy testing are shown in figure 13. Generally some slight non-linearity was observed during loading. During unloading the load-displacement curves returned to their origins, indicating that no permanent deformation of the specimens occurred on a macroscopic scale, which is one of the prerequisites for using Eq. 1 in calculating energy release rates.

For most specimens the test was continued after the onset of crack growth until the crack had extended over about 10 mm. In those cases crack growth was completely stable, i.e. the crack travelled slowly at a speed governed by the crosshead displacement of the test machine (type A in Fig. 13). In a few cases, however, the crack started to grow in a stable manner, but then suddenly extended very rapidly over a relatively large distance. These unstable crack extensions were accompanied by a significant load drop (type B in Fig. 13). Unstable crack growth sometimes occurred upon loading specimens for the first time. This behaviour was attributed to the presence of a blunt crack tip. For that reason the results of the first loading cycles were disregarded.

#### Fracture surfaces

The difference between stable and unstable crack growth could clearly be distinguished on the fracture surfaces of the specimens. Stable crack growth resulted in light grey coloured areas, whereas the unstable crack growth areas were much darker, see figure 14. When crack growth was stable during a



number of subsequent tests no macroscopic growth markings were visible on the fracture surface.

At a somewhat higher magnification the unstable crack growth areas showed a large number of growth markings, see figure 14, which suggests that crack growth occurred in a slip-stick manner. In addition, these markings indicate that the crack front was very wavy during unstable crack growth.

In all cases the fracture surfaces were macroscopically flat. Only occasionally could some broken fibres be observed, indicating that hardly any fibre bridging occurred during crack growth.

The colour differences on the fracture surfaces for stable and unstable fracture may have resulted from differences in the extent of micro yielding of the PEEK polymer, as suggested in reference 9: i.e. during stable crack growth the extent of plastic flow in the polymer is probably significantly larger than that during unstable crack growth.

#### Fracture energy

The results of the mode I fracture energy tests are listed in tables 1 to 5. In addition to the parameters measured directly from the test results (crack length, maximum load and compliance) the tables include the fitting parameters  $a_0$  and  $E_0$ , which were calculated using Eqs. 5 to 7.

For each specimen the average mode I fracture energy  $\bar{G}_{Ic}$  and the appropriate standard deviation were calculated. Finally, the last columns of tables 1 to 5 give the average mode I fracture energy  $(\bar{G}_{Ic})_{avg}$  and standard deviation per cooling rate. The latter data were calculated using all  $G_{Ic}$  values measured on specimens which were cooled at the same rate.

Figures 15 to 19 show plots of  $G_{Ic}$  versus crack length. Each of these figures shows the results of all three specimens cooled at the same rate. There was no systematic effect of crack length on  $G_{Ic}$ . In addition, from tables 1 to 5 it follows that the standard deviations for  $\bar{G}_{Ic}$  are relatively small. Thus, it can be concluded that the mode I fracture energy,  $G_{Ic}$ , is independent of crack length. This gives some confidence in the assumption that  $G_{Ic}$  can be regarded as a material property.



In figure 20  $(\bar{G}_{Ic})_{avg}$  is plotted versus cooling rate. This figure suggests that the mode I fracture energy, tends to increase with cooling rate in the range between 1 and 25 °C/min.

In figure 21 the average mode I fracture energy is shown together with the minimum and maximum fracture energies measured for each cooling rate. As can be seen, the scatterbands largely overlap each other, which throws doubt on the significance of the observed trend in figure 20.

The observed crack growth mode (stable/unstable) is also indicated in tables 1 to 5. The  $G_{Ic}$  data calculated from the results of tests during which crack growth was unstable did not differ systematically from the values calculated from tests during which stable crack growth occurred.

## 6.2 Mode II fracture energy

### Load-deflection curves

Typical load-deflection curves measured during tests on ENF specimens are presented in figure 22. The curves generally exhibited a linear behaviour up to 85-90% of the maximum load. Beyond this the slope of the curves gradually decreased with increasing load until a maximum was reached. The shape of the curves beyond maximum load fell into one of the following categories:

- A. On increasing the displacement, the load first decreased rather slowly until a large sudden load drop occurred at constant displacement (curve A in Fig. 22).  
This behaviour suggests that initially the crack grows slowly, but at an increasing rate, until it suddenly extends in an unstable manner and too fast for the test machine to follow.
- B. After reaching a maximum, the load decreased at a relatively high rate, but during crack growth a noticeable increase in displacement occurred (curve B in Fig. 22).
- C. The load decreased rather slowly on increasing the displacement until it started to increase again (curve C in Fig. 22).



This type of curve is most probably typical for a specimen in which a crack is growing at a rate that is fully governed by the crosshead speed of the testing machine, i.e. crack growth was completely stable until the crack tip reached the central loading pin. This type of load-deflection record was only observed for the 70 °C/min specimens.

#### Fracture energy

For all specimens the maximum load reached during the test was used in calculating the mode II interlaminar fracture energy. The compliances were determined from the linear sections of the load-deflection records. For each cooling rate an average mode II fracture energy,  $\bar{G}_{IIc}$ , was calculated. All results are summarized in table 6. The table also indicates the type of load-deflection curve observed during the test. Note that no data are included in table 6 for specimens 50B1 and 50B2, since those specimens were tested incorrectly.

The calculated  $G_{IIc}$  data are plotted versus the cooling rate in figure 23, which shows that:

- The scatter in the  $G_{IIc}$  data is relatively large.
- There is no systematic effect of cooling rate on  $G_{IIc}$ .

It is noteworthy that although the ENF specimens 10B1 to 10B5 were taken from areas of suspect laminate quality, this is not reflected in lower fracture energy values. This probably indicates that the defects, if any, were not at the midplane of the specimens.

The results of the tests on ENF specimens that were machined from the previously tested DCB specimens are given in table 7. For all specimens the load-deflection curve beyond the maximum load was of type A (see above). However, the magnitude of the sudden load drop was significantly smaller than that for the original ENF specimen. The  $G_{IIc}$  data are also plotted in figure 23. Although only two or three specimens per cooling rate were tested, these results suggest that:

- The fracture energy data and the scatter in the data are significantly smaller than those for the original ENF specimens.





- In the range of cooling rates between 1 to 30 °C/min,  $G_{IIc}$  tends to increase slightly with cooling rate. For higher cooling rates (70 °C/min)  $G_{IIc}$  tends to decrease again.

### Fracture surfaces

After testing the specimens were bent open until the specimen halves were completely separated. Photographs of the fracture surfaces of some of the original ENF specimens are shown in figures 24 and 25. The three different crack growth stages could easily be recognized:

1. Mode I precracking.
2. Mode II crack growth.
3. Crack growth during pulling open the specimens (in mode I).

For most specimens the mode I induced precracks appeared as light grey coloured areas, indicating that slow stable crack growth occurred during the creation of the cracks. Generally these cracks were highly asymmetrical. Moreover, the length of the precrack and the shape of the crack front varied significantly from one specimen to the other.

For some specimens the presence of dark grey coloured areas with typical growth markings indicated that unstable mode I crack growth occurred during the introduction of the precrack (specimens 1B5, 5B2, 5B3, 30B2, 30B3 and 70B3 to 70B5). The calculated fracture energies for these specimens were generally lower than those for specimens in which stable crack growth occurred during creation of the precrack. This suggests that  $G_{IIc}$  is strongly dependent on the type of precrack.

Below the precrack the fracture surfaces showed another dark grey coloured area, which represented the area over which mode II crack growth occurred. Within this area a transition from dark to light grey could be distinguished for specimens with type A load-deflection curves. It is assumed that this transition marked the position of the crack front at the transition of slow to fast crack growth.

The subsequent transitions from dark grey to light grey indicate the positions of the crack fronts at the end of mode II testing. The remaining part of the fracture surfaces were due to pulling open the specimens in a bending mode.



### 6.3 Iosupescu shear tests

For most specimens individual load-strains records were measured for the two gauge filaments ( $\epsilon^{+45}$  and  $\epsilon^{-45}$ ) on both sides of the notch. Figure 26 shows typical stress-strain curves measured during a test on one of the Iosupescu specimens (30C2). The strain values plotted in this figure are absolute values ( $\epsilon^{+45}$  and  $\epsilon^{-45}$  were of course opposite in sign). At the lower stress levels the two curves almost coincided. However, significant differences in strain response occurred in the plastic range.

The shear modulus, shear strength and strain to failure were determined from the recorded curves as described in section 5.5. The results are summarized in table 8 together with the dimensions of the specimens.

The shear modulus and shear strength data are plotted versus the cooling rate in figures 27 and 28, respectively. From these figures and table 8 it can be concluded that:

- The shear modulus and the shear strength tended to decrease slightly with increasing cooling rate.
- The shear strain to failure shows significant scatter (varying between 8 and 14 %). The data do not indicate that the cooling rate had a significant effect on the shear strain to failure.

In only a few cases did failure initiate at the notch root radius. In most specimens failure occurred close to the transition of notch root radius to notch flank, i.e. not at the minimum cross-section. Microscopic investigation of the notch root area did not reveal indications that this preferred failure location may have been due to improper machining of the notch: the transition of notch root to notch flank was very smooth without any discontinuity.

### 6.4 Fibre volume content

The results of the fibre volume determinations are summarized in table 9. As can be seen, the scatter in the data for samples originating from the same laminate is relatively large, in particular for the laminate programmed to cool at a rate of 5 °C/min. The average values suggest that the fibre volume fraction for the laminate cooled at 1 °C/min was significantly smaller than that for the laminates programmed to cool at 10, 30 and 70 °C/min.



## 7 DISCUSSION

### 7.1 The effect of cooling rate

The primary objective of this investigation was to determine the effect of cooling rate on some selected material properties of APC-2. It was observed that the mode I interlaminar fracture energy increased with cooling rate within the range investigated. However, the increase was limited to only 8 %. Tests on the End Notch Flexure specimens revealed conflicting results. The results of the "original" ENF specimens suggested that the mode II interlaminar fracture energy decreased slightly with increasing cooling rate, whereas the tests on the ENF specimens, machined from previously tested DCB specimens, indicated an increase of  $G_{IIc}$  by about 19 % on increasing the cooling rate from 1 to 70 °C/min. It is felt that the results of the ENF(DCB) specimens are more reliable for reasons to be discussed later. Finally, the shear modulus and the shear strength were observed to decrease very slightly with increasing cooling rate. All these results suggest that the brittleness of the material decreased slightly with increasing cooling rate.

The second objective was to check whether processing the material with a cooling rate below that specified by the manufacture (10 °C/min) would seriously degrade the mechanical behaviour. In that respect the results are encouraging. Cooling rates below 10 °C/min appear to have only a marginal effect on the mechanical properties. The most noticeable effect is a slight reduction of the interlaminar fracture energy.

During the first phase of this programme the effect of cooling rate on crystallinity was determined using Differential Scanning Calorimetry (Ref. 1). The results indicated that the crystallinity increases with decreasing cooling rate from 30 % at 0.5 °C/min to 37 % at 150 °C/min. Since a lower crystallinity can indeed be expected to result in a more ductile behaviour, the present results seem to be in agreement with those of the crystallinity measurements. It should, however, be noted that the scatter in both crystallinity and mechanical properties data was significant, whereas the effect of cooling rate itself was rather small. Any attempt to correlate the results of the two investigations in more detail would therefore be very questionable. This is particularly because cooling rate not only affects the



degree of crystallinity in the laminates, but also the magnitude of the internal stresses and the fibre volume fraction.

Berglund (Ref. 10) also investigated the effect of crystallinity on fracture energy of APC-2. During that investigation specimens were produced with cooling rates varying between 15 and 10000 °C/min. The results showed that the cooling rate had a pronounced effect on  $G_{Ic}$ . For the highest cooling rates  $G_{Ic}$  was found to be about 2.1 kJ/m<sup>2</sup> (crystallinity 0 %), whereas at a cooling rate of 15 °C/min  $G_{Ic}$  was only 0.98 kJ/m<sup>2</sup> (crystallinity 33 %). The latter value of  $G_{Ic}$  is significantly smaller than that measured during the present investigation. The reason for this discrepancy is unknown. In another publication (Ref.3), however, the same author described results of an investigation into the effect of deformation rate on  $G_{Ic}$ . In that publication values ranging from 1.58 and 2.17 kJ/m<sup>2</sup> are reported for laminates cooled at 40 °C/min, which are much more in agreement with the present test results.

## 7.2 Evaluation of the test methods

### Mode I fracture energy

Recently an international round robin programme was performed with the objective to establish an ASTM standard method for mode I interlaminar fracture energy testing (Ref. 11). The data contained in the programme were generated on AS4/PEEK laminates and may thus serve as a comparison basis for the present test results. But first some comments on the recommended test procedure will be made.

The tests were done on DCB specimens with different kind of inserts to simulate a precrack. In contrast with the presently applied procedure the test was continuous, i.e. after the onset of crack growth the crack was allowed to grow over the total length of the specimen (no loading/unloading cycles). At several stages during the tests the momentary crack length and load were measured.

Based on the results of the round robin programme it was recommended to calculate  $G_{Ic}$  for crack initiation from the load at which the load-displacement record starts to deviate from linearity, since this gives a



conservative value and since this value for  $G_{Ic}$  was least dependent upon the thickness of the insert.

However, in the first instance one may wonder whether a  $G_{Ic}$  value based upon the load at which onset of non-linearity occurs has any practical significance, in particular when it is known that the onset of non-linearity is not caused by the onset of crack growth. In addition, the determination of the load at which the record starts to deviate from linearity is rather arbitrary, since the transition occurs very gradually.

Calculating  $G_{Ic}$  initiation values from the load at which delamination onset occurs is undoubtedly the most realistic approach. However, the round robin programme showed that this value is dependent upon the type and thickness of the polyimide insert.

The present test results indicate that reproducible  $G_{Ic}$  initiation values can be obtained from DCB specimens when they contain mechanically induced precracks. This can be done simply by applying one loading/unloading cycle during which the artificial precrack is allowed to grow for about 10 mm. It is felt that the presently applied test procedure (with several loading-unloading cycles) is to be preferred when  $G_{Ic}$  initiation values have to be determined, since multiple data are obtained on a single specimen. However, a continuous test (without unloading) may yield a more reliable R-curve of the material. It would be interesting to compare both test procedures on specimens taken from the same laminate.

Reference 12, which details the contribution of the Aeronautical Research Institute of Sweden to the round robin programme, shows that the so-called  $G_{Ic}$  for propagation was dependent on crack length. The values found at relatively small crack lengths (1.7 - 2.1 kJ/m<sup>2</sup>) agree reasonably well with the presently found  $G_{Ic}$  initiation data. With increasing crack length  $G_{Ic}$  for propagation tended to a constant value of about 1.4 - 1.6 kJ/m<sup>2</sup>.

In reference 9,  $G_{Ic}$  tests are described using the same type of specimen and the same material as were used during the present investigation. The material was cooled at a rate of about 20 °C/min. The average  $G_{Ic}$  value was found to be 1.95 kJ/m<sup>2</sup>, which also is in agreement with the present test results. From the results of that investigation it was also concluded that when unstable



crack growth occurred during the test,  $G_{Ic}$  was larger than when crack growth was stable. The higher  $G_{Ic}$  values were attributed to crack tip blunting, resulting from either a local increase in the resin concentration at the crack tip or the occurrence of some fibre bridging during the previous crack growth increment. During the present investigation such a difference was not observed. The absence of an effect of crack growth type may well have been due to the fact that unstable crack growth was always preceded by a small amount of stable crack growth, i.e. cracks always initiated in a stable manner.

#### Mode II fracture energy

Earlier in this chapter it was stated that the results of the tests on the ENF(DCB) specimens were probably more reliable than those of the original ENF specimens. This statement is based on the following arguments:

1. The precrack in the original ENF specimen was not well defined, as already described in section 6.2.
2. The original ENF specimens were asymmetrically positioned in the loading fixture.
3. The ENF(DCB) specimens yielded lower energy values.

The first two arguments indicate that the tests were not properly performed, which may give doubts as to the reliability of the results.

The fracture energy measured during a test may be expected to increase with the bluntness of the crack tip. The sharp crack tip in the ENF(DCB) specimens, which all had mechanical precracks, is most probably the main cause that those specimens gave low fracture energies values. The high fracture energies measured with the original ENF specimens may have been due to the fact that in most of these specimens the mechanical precrack did not extend over the full width of the crack front, i.e. over part of the crack front the crack tip was still relatively blunt. In addition, the large amount of scatter in the fracture energy data of the original ENF specimens may have been due to large differences in crack tip geometry in those specimens.

In Ref. 13 ENF specimens were used to determine the effect of displacement rate on  $G_{IIc}$  for APC-2. The specimens were produced with a cooling rate of about 40 °C/min. The geometry of the ENF specimens was essentially the same as that used for the present investigation, including the Kapton film at the laminate mid-plane. Before testing the specimens were precracked by pushing a



razor blade into the tip of the artificial precrack. It was found that at relatively small displacement rates  $G_{IIc}$  was about constant:  $G_{IIc} = 1.9 \text{ kJ/mm}^2$ , which is in between the values found for the original ENF specimens and of the ENF(DCB) specimens.

#### Iosupescu shear test

The strain gauge results showed that in the elastic range the  $+45^\circ$  and  $-45^\circ$  strains were almost equal, indicating that a state of pure shear existed at the location of the gauges. This means that the test fixture performed well and that the procedures used to prepare and install the specimens were probably sufficiently accurate. However, it does not prove that the measured shear strains were solely due the applied shear force. As pointed out in references 14 and 15, shear strains may also occur due to twisting of the specimen during loading: in particular, the specimen configuration with fibres parallel to the loading line was experimentally shown to be prone to twisting, i.e. much more than specimens with fibres perpendicular to the loading line. It was suggested that this was due to the hardness of the specimen edges in contact with the loading fixture, resulting in concentrated contact areas and an uneven load distribution in both the longitudinal (x) and transverse (z) direction. This phenomenon could easily result in a load eccentricity in the transverse directions, which will introduce torsional strains into the specimen. According to the authors in references 14 and 15, the scatter generally observed in the shear modulus data generated with the Iosupescu test fixture can be attributed largely to differences in the extent of twisting.

For the present tests the standard deviations in the shear modulus data were between 1.9 and 4.1 % of the average values. This kind of standard deviation is normally encountered in composite material properties testing programmes, and may reflect the inherent variability in mechanical properties of this type of material. In other words, the variability presently observed in shear modulus data is not necessarily due to shortcomings of the test method. Nevertheless, it is recommended that in future the Iosupescu shear specimens are instrumented with strain gauges on both sides in order to check for the occurrence of twisting.



In reference 14 it was also shown that the shear stress distribution was not entirely uniform over the line between the notch roots. For a specimen with fibres parallel to the loading line the shear stress at the centre of the specimen was shown to be about 1.2 times the average shear stress. Therefore, a correction factor (CF) should be applied to the experimentally determined shear moduli. The value of this correction factor is slightly dependent on the degree of material anisotropy, as shown in Ref.14:

$$CF = 1.036 - 0.125 \log \left( \frac{E_x}{E_y} \right) \quad (15)$$

However, the value of the correction factor to be applied also depends on the positions and dimensions of the strain gauges. In reference 14 stacked strain gauges were positioned exactly at the centre of the specimen, whereas in our tests the gauges were positioned symmetrically with respect to the centreline of the specimen. Detailed FEM analysis would be necessary to determine the appropriate correction factor for the present test results, but this was outside the scope of the programme. For future testing programmes the use of stacked strain gauges is recommended.

The results of the tests showed that failure generally occurred slightly removed from the notch root. The location of failure was not the same for all specimens, although for most specimens it occurred close to the transition of notch root radius to notch flank. The cause of the unexpected failure location is not known. It may have been surface irregularities or damage (small cracks) at the edge surfaces created during machining of the notches, since the edges were not carefully inspected before the tests. However, the failure location may also indicate that the stress state at the notch tip is not significantly more severe than that along the notch flanks. In particular, the presence of tensile stresses along the notch flanks may have promoted failure at these locations. Since failure was not initiated at the notch root radius, little value should be attached to the data giving shear strain to failure. In fact, the scatter observed in  $\gamma_f$  may have been due to the variation in failure location. On the other hand the shear strength is probably less sensitive to the failure location, because there is hardly any strain hardening before failure occurs. The shear strength values measured during the present investigation (82 - 86 MPa) agree reasonably well with the





values found for IM6/APC-2 in Ref. 16 using slotted compression test specimens ( $\tau_f = 88.5$  Mpa).

## 8 CONCLUSIONS

The effect of cooling rate on some mechanical properties of AS4/APC-2 was investigated in the range from 1 to 70 °C/min.

The critical energy release rate for mode I interlaminar crack initiation (or mode I fracture energy,  $G_{Ic}$ ) was determined using a prismatic Double Cantilever Beam specimen. The results of the tests showed that:

- $G_{Ic}$  is independent of crack length.
- $G_{Ic}$  tends to increase with cooling rate.

The critical energy release rate for mode II crack initiation was measured with End Notch Flexure specimens. From the results of specimens machined from previously tested DCB specimens it is concluded that:

- $G_{IIc}$  increases with cooling rate.

Another test series on ENF specimens, with moulded-in precracks, showed a large amount of scatter in the calculated  $G_{IIc}$  data and a non-systematic effect of cooling rate on  $G_{IIc}$ . The scatter is attributed to the large differences in crack geometry in these specimens.

The interlaminar shear properties were determined with the Iosupescu test method. The results indicated that:

- The shear modulus and the shear strength decrease slightly with increasing cooling rate.

The overall conclusions can be summarized as follows:

- (1) Within the range investigated, the brittleness of the material increases slightly with decreasing cooling rate.
- (2) Decreasing the cooling rate below the minimum value specified by the material supplier (10 °C/min) will most probably not lead to an abrupt or substantial degradation of the mechanical performance.



## 9 REFERENCES

1. Hoeven, W. van der, Effect of Cooling Rate on the Crystallinity of APC2, NLR TP 93287 L.
2. Mall, S.; Law, G.E.; Katouzian, M., Loading Rate Effect on Interlaminar Fracture Energy of a Thermoplastic Composite, Journal of Composite Materials, Vol. 21, No. 6, pp. 569 - 579, 1987.
3. Berglund, L.A.; Johanneson, T.R., Effect of Deformation Rate on the Mode I Interlaminar Crack Propagation in Carbon Fiber/PEEK Composites. In: Fracture Toughness of Carbon Fiber/PEEK Composites, Linkoping Studies in Science and Technology, Dissertation No. 159, 1987.
4. Nosupescu, N., New Accurate Method for Single Shear Testing of Metals, Journal of Materials, Vol. 23, No. 1, pp. 105-110.
5. Walrath, D.E.; Adams, D.F., Analysis of the Stress State in an Iosupescu Shear Test Specimen, Department report UWME-DR-301-102-1, University of Wyoming, Technical Report NASA-Langley Research Center, Grant No. NAG-1-272, June 1983.
6. Walrath, D.E.; Adams, D.F., Verification and Application of the Iosupescu Shear Test Method, Department Report UWME-DR-401-103-1, University of Wyoming, Technical Report NASA-Langley Research Center, Grant No. NAG-1-272, June 1984.
7. ACEE Composites Project Office, Standard Tests for Toughened Resin Composites - Revised Edition, NASA Reference Publication 1092, 1983.
8. Russell, A.J., On the Measurement of Mode II Interlaminar Fracture Energies, Materials Report 82-0, Defense Research Establishment Pacific Victoria, B.C, Canada, Dec. 1982.
9. Hines, P.J.; Brew, B, The Fracture Behaviour of Carbon Reinforced Poly(Ether Etherketone), Composite Science and Technology, Vol. 33, 1988, pp. 35-71.
10. Talbott, M.F.; Springer, G.E.; Berglund, L.A., Effects of Crystallinity on the Mechanical Properties of PEEK Polymer and Graphite Fiber Reinforced PEEK. In: Fracture Toughness of Carbon Fiber/PEEK Composites, Linkoping Studies in Science and Technology, Dissertation No. 159, 1987.
11. O'Brian, K.; Martin, R., Experiences in Round Robin Testing of AS4/PEEK Thermoplastic Composites using the Double Cantilever Beam Specimen. In: Composite Testing and Standardisation, ECCM-CTS Conference, Amsterdam, September 8-10, 1992.



12. Olsson, R., Mode I Interlaminar Fracture Toughness of Carbon/PEEK, Participation in an International Round Robin Program, FFA TN 1990-41, The Aeronautical Research Institute of Sweden, Stockholm, 1990.
13. Smiley, A.J.; Pipes, R.B., Rate Sensitivity of Mode II Interlaminar Fracture Toughness in Graphite/Epoxy and Graphite/PEEK Composite Materials, Composites Science and Technology Vol. pp. 1-15, 1987.
14. Morton, J.; Ho, H.; Tsai, Y. e.o., An Evaluation of the Iosupescu Specimen for Composite Materials Shear Property Measurement, Journal of Composite Materials, Vol. 26, No. 5, pp. 708 - 749, 1992.
15. Lee, S.; Munro, M., Evaluation of Testing Techniques for the Iosupescu Shear Test for Advanced Composite Materials, Journal of Composite Materials, Vol. 24, No. 4, pp. 419 - 440, 1990.
16. Frijns, R.H.W.M.; Hart, W.G.J. 't, Basic Material Qualification of the advanced Carbon Fibre Composite T800H/5245C and IM6/APC-2, NLR TR 89047 L, 1989.



Table 1 Results of  $G_{Ic}$  tests for cooling rate: 1 °C/min

Spec. nos.	Measured data			Fit parameters		Fracture energy		
	Crack length	Max. load	Compliance	$a_o$	$E_o$	$G_{Ic}$	$\bar{G}_{Ic}$	$(\bar{G}_{Ic})_{avg}$
	a	$P_{max}$	C				(s.d.)	(s.d.)
	mm	N	mm/N	mm	MPa	J/m <sup>2</sup>	J/m <sup>2</sup>	J/m <sup>2</sup>
1A1	54.9	98.0	0.151	13.73	147982	1775	1739 (62)	
	64.2	81.6	0.236			1640		
	75.9	71.1	0.370			1703		
	87.5	67.7	0.525			1734*		
	107.2	53.3	0.985			1842*		
	132.3	42.4	1.180			1743		
1A2	70.7	81.2	0.281	8.42	139031	1867	1877 (45)	1767 (104)
	83.7	69.4	0.457			1884		
	95.9	61.5	0.652			1927		
	106.6	54.0	0.909			1827		
	117.9	49.7	1.205			1877		
	127.4	45.2	1.568			1811		
	139.6	42.9	1.988			1946		
1A3	59.6	90.7	0.188	8.37	130909	1833	1691 (74)	
	70.0	75.9	0.292			1745		
	79.7	66.6	0.431			1724		
	89.1	58.8	0.610			1666		
	101.1	50.9	0.854			1592		
	112.6	46.0	1.188			1608		
	124.7	43.1	1.542			1720		
	134.3	39.2	1.975			1648		

\* Unstable crack growth after initiation.



Table 2 Results of  $G_{Ic}$  tests for cooling rate: 3.7 °C/min.

Spec. nos.	Measured data			Fit parameters		Fracture energy		
	Crack length a	Max. load $P_{max}$	Compliance C	$a_0$	$E_0$	$G_{Ic}$	$\bar{G}_{Ic}$ (s.d.)	$(\bar{G}_{Ic})_{avg}$ (s.d.)
	mm	N	mm/N	mm	MPa	J/m <sup>2</sup>	J/m <sup>2</sup>	J/m <sup>2</sup>
5A1	55.9	95.3	0.197	21.20	162358	1729	1769 (54)	
	66.2	84.4	0.245			1839		
	78.0	69.5	0.407			1674		
	89.5	63.0	0.590			1772*		
	125.2	46.4	1.519			1796		
	139.6	41.9	2.070			1803*		
5A2	80.5	66.8	0.444	14.96	150193	1693	1858 (123)	1799 (79)
	92.3	61.6	0.642			1860		
	104.6	54.4	0.914			1840*		
	138.2	43.9	2.047			2040		
5A3	57.1	96.2	0.173	13.52	149017	1875	1792 (44)	
	68.8	79.5	0.281			1807		
	81.0	67.7	0.451			1785		
	94.95	59.4	0.666			1745		
	103.1	52.9	0.892			1717		
	114.5	49.0	1.193			1802		
	127.6	44.1	1.603			1801		
	139.2	40.6	2.139			1801		

\* Unstable crack growth after initiation.



Table 3 Results of  $G_{Ic}$  tests for cooling rate: 6.5 °C/min.

Spec. nos.	Measured data			Fit parameters		Fracture energy		
	Crack length	Max. load	Compliance	$a_o$	$E_o$	$G_{Ic}$	$\bar{G}_{Ic}$	$(\bar{G}_{Ic})_{avg}$
	a	$P_{max}$	C				(s.d.)	(s.d.)
	mm	N	mm/N	mm	MPa	J/m <sup>2</sup>	J/m <sup>2</sup>	J/m <sup>2</sup>
10A1	57.9	97.3	0.183	13.91	144059	1978	2027 (34)	
	67.8	85.2	0.273			2037		
	78.9	75.1	0.423			2097		
	90.1	65.1	0.599			2024		
	100.2	58.2	0.850			1985		
	110.5	53.6	1.104			2025		
	120.7	49.4	1.413			2037		
	131.1	45.5	1.764			2031		
10A2	57.5	91.0	0.182	11.82	143826	1718	1796 (60)	1882 (173)
	66.2	81.2	0.236			1781		
	78.0	70.8	0.417			1848		
	87.1	61.9	0.580			1742		
	97.3	55.5	0.767			1729		
	108.5	52.1	1.050			1879		
	117.7	47.2	1.320			1800		
	127.8	44.4	1.640			1871		
10A3	57.1	92.6	0.179	17.68	157539	1780	1815 (237)	
	66.2	78.5	0.275			1672		
	77.5	67.9	0.417			1672		
	86.9	59.5	0.603			1585		
	96.5	54.8	0.777			1637*		
	123.6	49.8	1.458			2160		
	136.6	46.4	1.913			2200*		

\* Unstable crack growth after initiation.



Table 4 Results of  $G_{Ic}$  tests for cooling rate: 24 °C/min.

Spec. nos.	Measured data			Fit parameters		Fracture energy		
	Crack length	Max. load	Compliance	$a_0$	$E_0$	$G_{Ic}$	$\bar{G}_{Ic}$	$(\bar{G}_{Ic})_{avg}$
	a	$P_{max}$	C				(s.d.)	(s.d.)
	mm	N	mm/N	mm	MPa	J/m <sup>2</sup>	J/m <sup>2</sup>	J/m <sup>2</sup>
30A1	61.0	85.4	0.227	17.19	151735	1785	1985 (134)	
	69.9	76.6	0.326			1846		
	80.9	68.7	0.500			1942		
	91.0	63.5	0.676			2065		
	101.5	55.0	0.909			1900		
	111.7	52.6	1.218			2008		
	121.7	47.8	1.525			2029		
	131.8	46.4	1.875			2224		
30A2	60.8	87.4	0.225	17.88	154314	1845	1926 (69)	1917 (113)
	70.2	77.6	0.325			1893		
	80.6	68.2	0.493			1884		
	91.3	60.3	0.688			1853		
	101.6	55.5	0.929			1921		
	111.4	51.5	1.188			1967		
	122.6	47.4	1.525			1995		
	132.8	44.6	1.889			2057		
30A3	62.4	83.9	0.250	20.51	159319	1781	1840 (71)	
	71.8	74.4	0.350			1804		
	80.7	66.5	0.508			1784		
	91.4	60.3	0.696			1848		
	102.5	52.8	0.964			1750		
	112.6	49.9	1.200			1860		
	123.2	46.8	1.155			1939		
	132.4	43.9	1.889			1957		

\* Unstable crack growth after initiation.



Table 5 Results of  $G_{Ic}$  tests for cooling rate 72 °C/min.

Spec. nos.	Measured data			Fit parameters		Fracture energy		
	Crack length a	Max. load $P_{max}$	Compliance C	$a_0$	$E_0$	$G_{Ic}$	$\bar{G}_{Ic}$ (s.d.)	$(\bar{G}_{Ic})_{avg}$ (s.d.)
	mm	N	mm/N	mm	MPa	J/m <sup>2</sup>	J/m <sup>2</sup>	J/m <sup>2</sup>
70A1	45.7	120.2	0.103	15.01	151735	1986	2011 (65)	
	56.5	97.4	0.167			1914		
	66.9	83.2	0.273			1904		
	77.6	75.0	0.403			2039		
	88.7	66.2	0.594			2037		
	99.0	59.4	0.805			2026		
	108.5	55.0	1.053			2065		
	118.4	51.3	1.344			2119*		
70A2	46.6	114.6	0.106	13.59	153496	1906	1883 (55)	1916 (87)
	57.3	92.6	0.178			1817		
	67.9	81.6	0.288			1929		
	77.5	69.5	0.417			1794		
	88.3	62.3	0.600			1842		
	97.9	58.0	0.779			1946		
	108.3	52.0	1.080			1895		
	118.1	48.0	1.361			1938		
70A3	47.6	108.0	0.109	10.76	147238	1814	1854 (34)	
	57.2	91.9	0.183			1845		
	66.8	49.7	0.275			1863		
	77.8	68.0	0.432			1810		
	88.7	60.8	0.617			1857		
	97.6	55.2	0.821			1836		
	107.7	51.0	1.091			1897		
	118.1	46.8	1.430			1911		

\* Unstable crack growth after initiation.





Tabel 6 Results of  $G_{IIc}$  tests on original ENF specimens

Spec. nos.	Dimensions			Measured data				Fracture Energy	
	Width	Thick-ness		Crack length	Compliance	Max. load	Curve type	$G_{IIc}$	$\bar{G}_{IIc}$
	W	t	z	a	$C \cdot 10^3$	$P_c$			(s.d.)
	mm	mm	mm	mm	m/N	N	J/m <sup>2</sup>	J/m <sup>2</sup>	
1B1	20.04	3.17	6.0	19.5	2.05	1639.6	A	3132	2551 (339)
1B2	20.04	3.16	5.5	20.5	2.13	1362.8	B	2427	
1B3	20.02	3.15	5.0	20.2	2.12	1366.4	B	2377	
1B4	20.02	3.14	4.0	20.8	2.11	1424.0	B	2684	
1B5	20.04	3.13	5.0	21.5	2.17	1223.2	B	2135	
5B1	20.03	3.15	6.0	20.0	2.18	1252.8	A	2023	1986 (169)
5B2	20.02	3.13	8.0	19.7	2.13	1172.8	B	1693	
5B3	20.02	3.13	7.0	20.5	2.04	1246.0	A	1945	
5B4	20.04	3.14	5.0	19.8	2.01	1372.4	A	2203	
5B5	20.04	3.16	5.0	19.8	1.90	1367.6	A	2068	
10B1	20.03	3.07	5.5	19.0	2.22	1508.2	A	2757	2527 (274)
10B2	20.05	3.03	6.0	18.0	2.23	1440.8	A	2314	
10B3	20.04	3.04	4.0	19.3	2.17	1559.6	A	2952	
10B4	20.02	3.04	6.0	18.3	2.24	1420.0	A	2323	
10B5	20.05	3.05	3.5	19.2	2.22	1364.0	A	2290	
30B1	20.04	3.05	9.0	19.8	2.25	1438.0	A	2707	2369 (190)
30B2	20.04	3.04	10.0	19.3	2.20	1374.4	A	2324	
30B3	20.03	3.05	1.05	20.7	2.35	1281.2	B	2402	
30B4	20.04	3.10	7.5	19.8	2.06	1334.0	A	2133	
30B5	20.04	3.10	7.0	20.0	2.06	1368.8	A	2281	
70B3	20.02	3.03	0.0	20.0	2.16	1155.2	C	1705	1894 (135)
70B4	19.76	3.01	5.5	20.8	2.35	1145.6	C	1960	
70B5	20.03	3.03	4.5	22.3	2.37	1108.0	C	2016	



Table 7 Results of  $G_{IIc}$  tests on ENF(DCB) specimens

Spec. nos.	Dimensions		Measured data				Fracture Energy	
	Width	Thick-ness	Crack-length	Compli-ance	Max. load	Curve type	$G_{IIc}$	$\bar{G}_{IIc}$
	W mm	t mm	a mm	$C \cdot 10^3$ m/N	$P_c$ N		J/m <sup>2</sup>	J/m <sup>2</sup>
1A1	20.00	3.21	20	2.25	1042.2	A	1447	1467
1A3	20.00	3.18	20	2.16	1078.2	A	1487	
5A2	20.04	3.14	20	2.23	1070.2	A	1509	1543
5A3	20.03	3.12	20	2.22	1095.8	A	1576	
10A1	20.05	3.15	20	2.27	1163.8	A	1816	1757
10A2	20.04	3.12	20	2.25	1130.0	A	1698	
30A1	20.01	3.07	20	2.32	1168.4	A	1874	1811
30A2	20.03	3.07	20	2.27	1177.4	A	1860	
30A3	20.04	3.07	20	2.32	1112.6	A	1697	
70A2	20.04	3.05	20	2.32	1076.8	A	1590	1575
70A3	20.03	3.03	20	2.38	1053.2	A	1561	



Table 8 Results of Iosupescu shear tests

cooling rate (°C/min)	specimen nos.	dimensions		mechanical properties				
		width	thick-ness	$\tau^f$	$\tau^f_{avg}$ (s.d.)	G	$G_{avg}$	$\gamma^f$
		(mm)	(mm)	(MPa)	(MPa)	(MPa)	(MPa)	(%)
1	1C1	11.63	3.09	86.8	85.8 (0.8)	4118	4129	10.40
	1C2	11.62	3.08	86.3		4222		10.69
	1C3	11.62	3.06	86.0		4171		11.44
	1C4	11.62	3.04	84.4		-		-
	1C5	11.61	3.02	85.2		4003		8.86
3.7	5C1	11.61	3.12	83.4	84.3 (0.9)	4020	4238	8.20
	5C2	11.58	3.11	85.2		4281		11.62
	5C3	11.61	3.10	85.6		4279		12.29
	5C4	11.61	3.09	83.6		4372		9.29
	5C5	11.61	3.08	83.9		-		-
6.5	10C1	11.59	3.03	88.4	85.7 (1.5)	-	4078	-
	10C2	11.59	3.03	84.0		3997		-
	10C3	11.58	3.03	85.5		4218		12.88
	10C4	11.58	3.04	85.0		3987		12.03
	10C5	11.60	3.05	85.3		4111		11.54
24	30C1	11.61	3.04	85.2	84.3 (0.9)	-	3945	-
	30C2	11.65	3.04	84.9		3703		10.51
	30C3	11.65	3.04	84.8		3899		11.59
	30C4	11.65	3.02	82.9		4130		9.36
	30C5	11.65	3.03	83.7		4047		10.58
72	70C1	11.61	3.00	81.2	82.1 (1.1)	3889	3878	11.73
	70C2	11.61	2.98	-		-		-
	70C3	11.61	2.99	80.9		3778		12.04
	70C4	11.61	2.98	83.8		3982		10.49
	70C5	11.61	2.97	82.3		3862		13.76



Table 9 Results of fibre volume fraction measurements.

Cooling rate (°C/min)	Specimen nos.	Fibre volume fraction	
		$\nu_f$ (%)	Average $\nu_f$ (s.d.) (%)
1	1E1	55.7	56.8 (0.7)
	1E2	57.3	
	1E3	57.2	
	1E4	57.4	
	1E5	56.6	
3.7	5E1	67.6	60.6 (4.2)
	5E2	58.8	
	5E3	59.7	
	5E4	60.3	
	5E5	56.5	
6.5	10E1	59.8	60.2 (0.5)
	10E2	59.7	
	10E3	60.1	
	10E4	60.8	
	10E5	60.6	
24	30E1	60.7	62.6 (1.2)
	30E2	62.6	
	30E3	62.4	
	30E4	64.0	
	30E5	63.3	
72	70E1	60.0	61.5 (1.0)
	70E2	61.5	
	70E3	61.7	
	70E4	61.7	
	70E5	62.7	

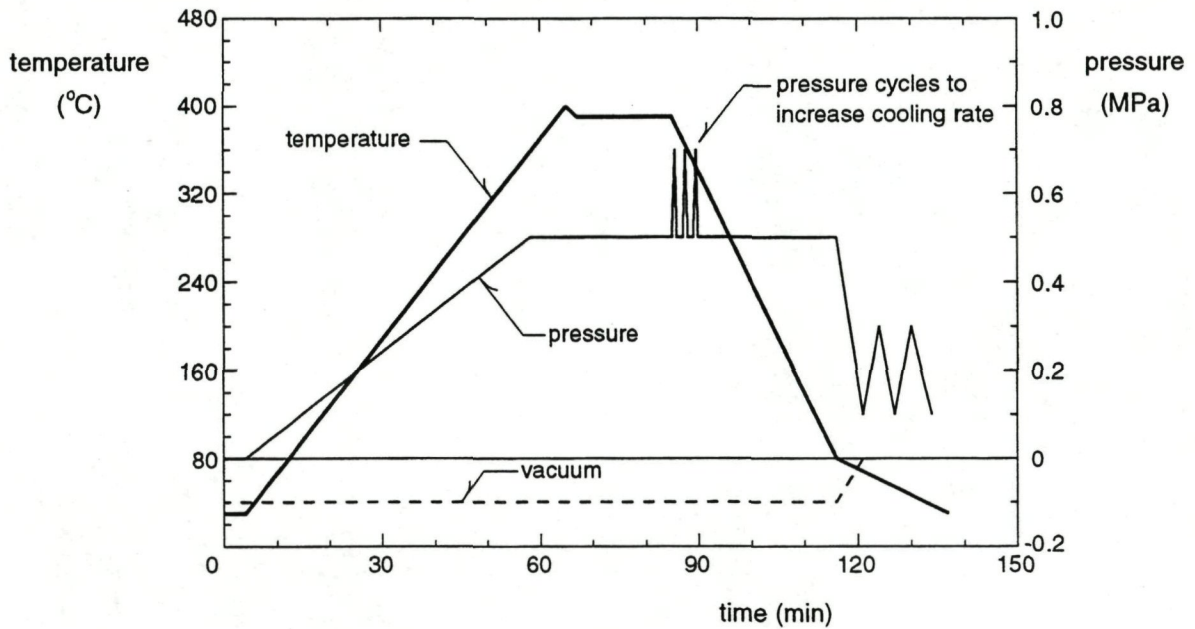


Fig. 1 Temperature and pressure cycle applied during autoclave moulding.

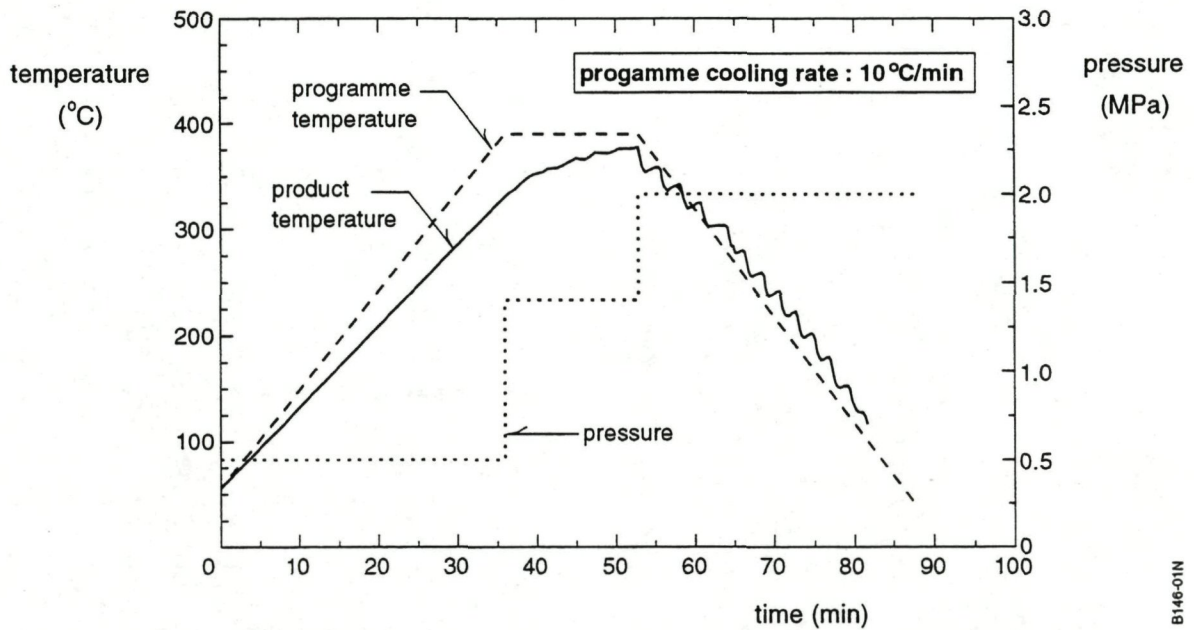


Fig. 2 Temperature and pressure cycle applied during press forming. The solid line shows the response of the APC-2 sheet

B146-01N

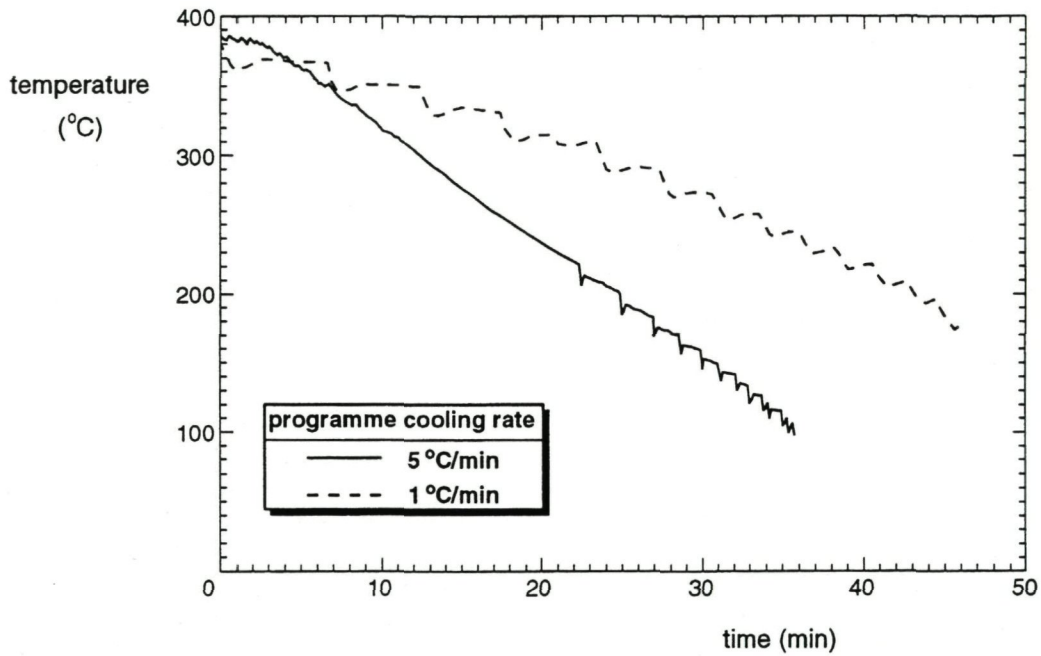


Fig. 3 Cooling curves measured during press moulding of the laminates at programmed rates of 1 and 5 °C/min

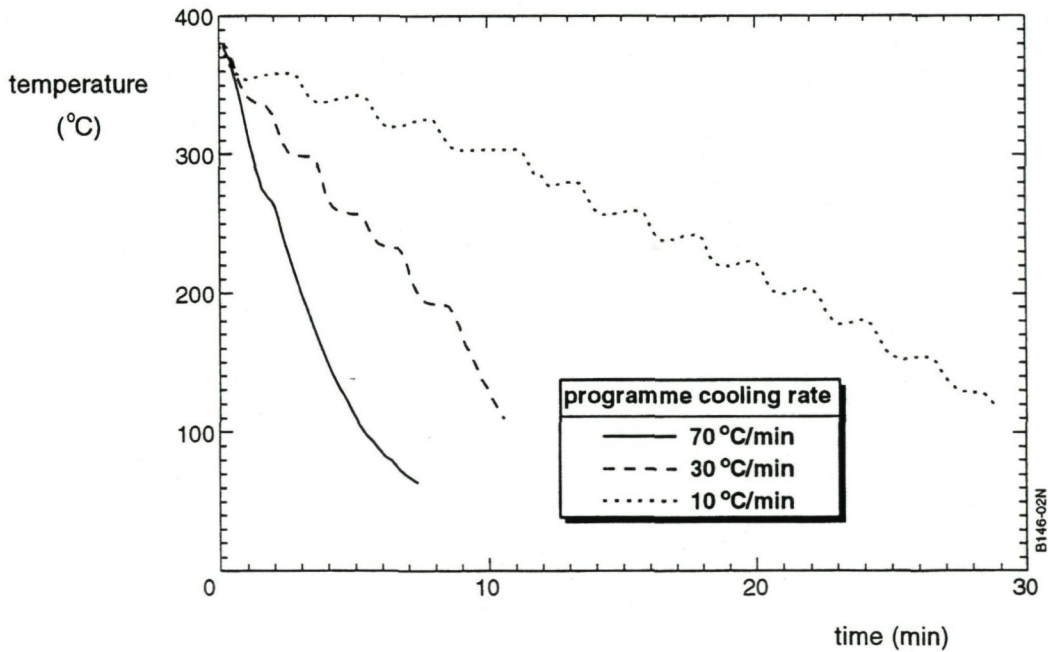


Fig. 4 Cooling curves measured during press moulding of the laminates at programmed rates of 10, 30 and 70 °C/min

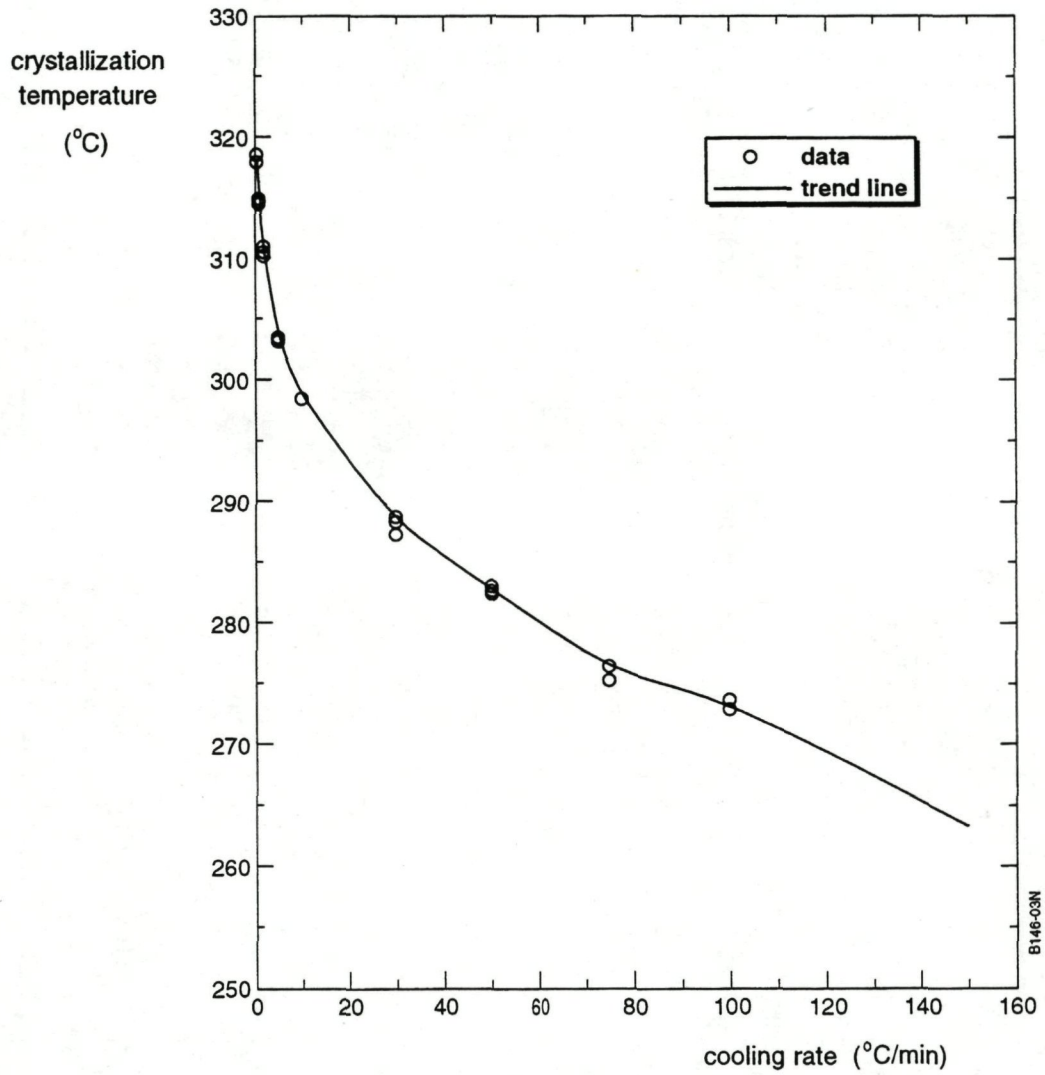


Fig. 5 Crystallization temperature for APC-2 as a function of cooling rate (Ref. 1)

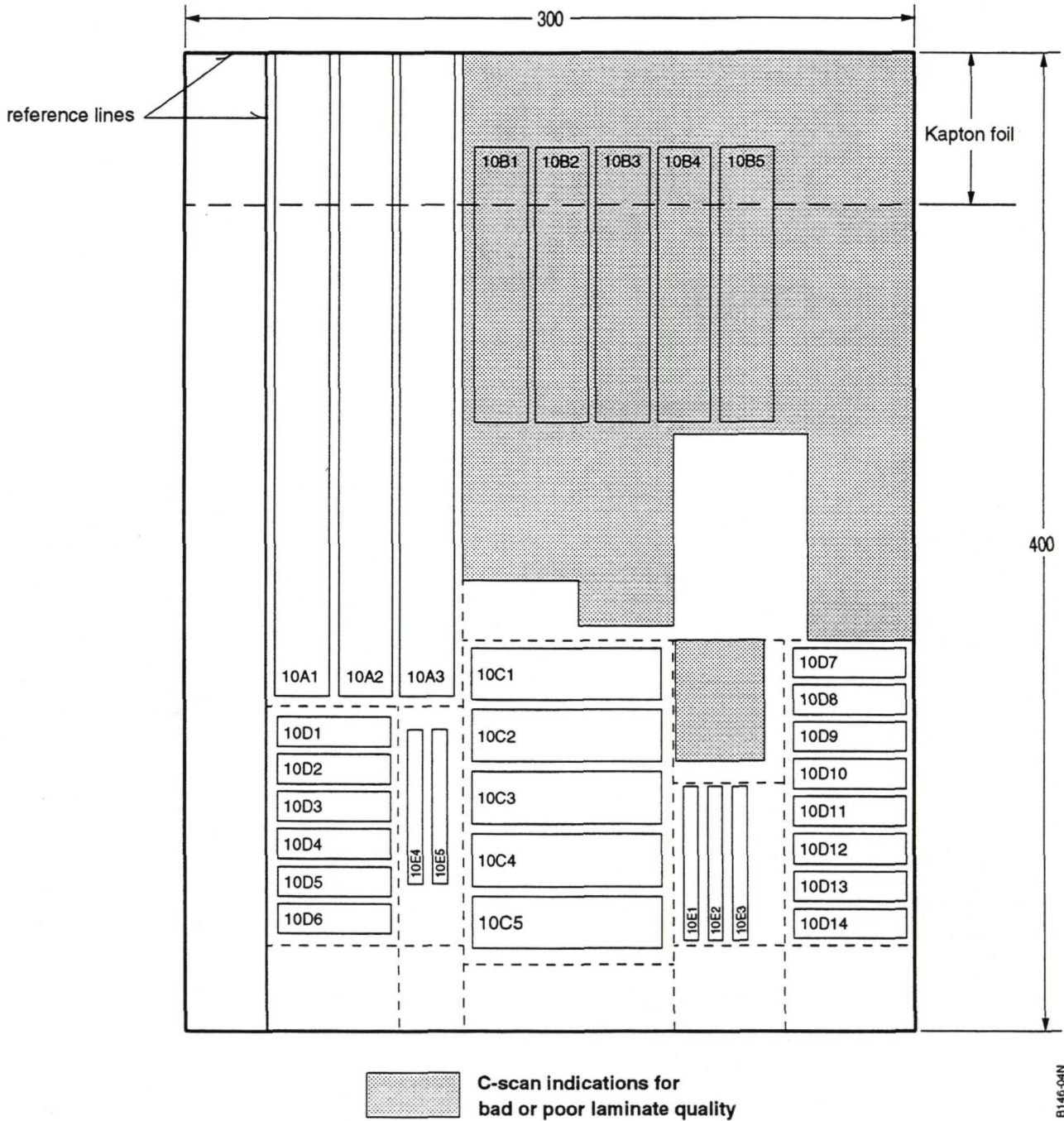


Fig. 6 Cut-up scheme for APC-2 sheet programmed to cool at a rate of 10 °C/min

B146-04N



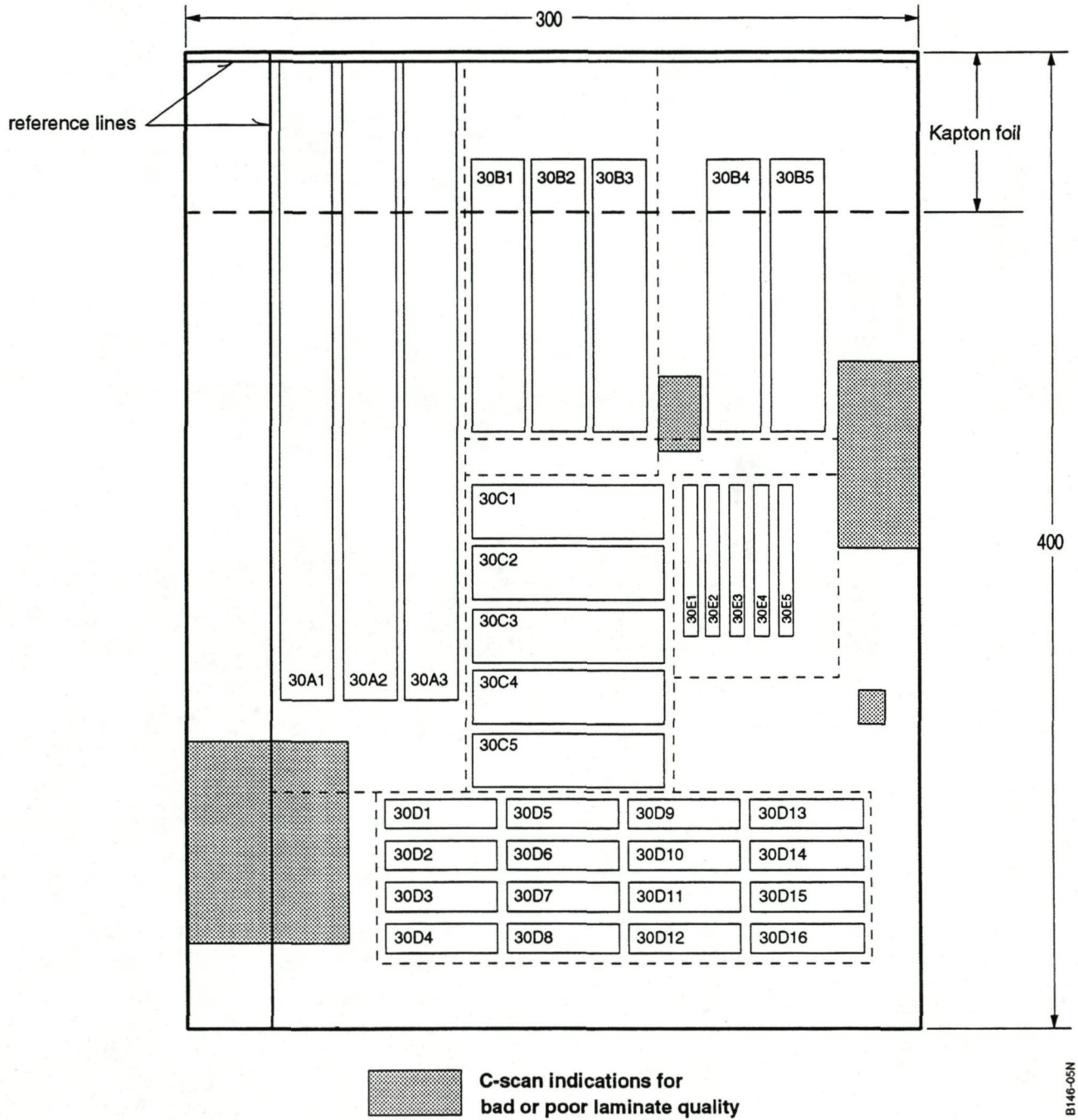
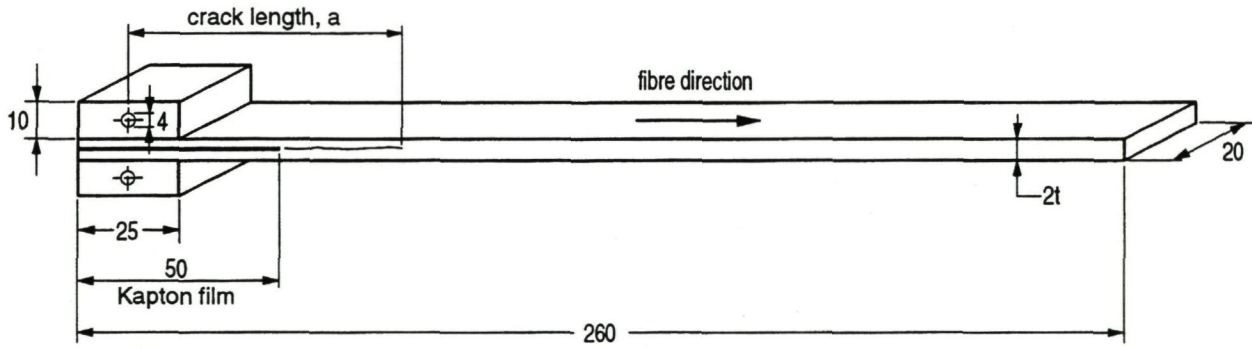
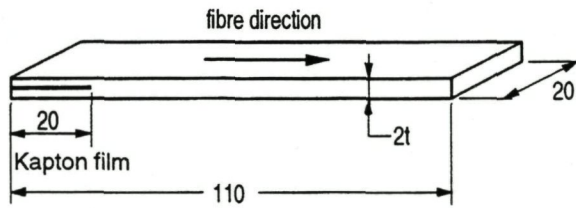


Fig. 7 Cut-up scheme for APC-2 sheet programmed to cool at a rate of 30 °C/min



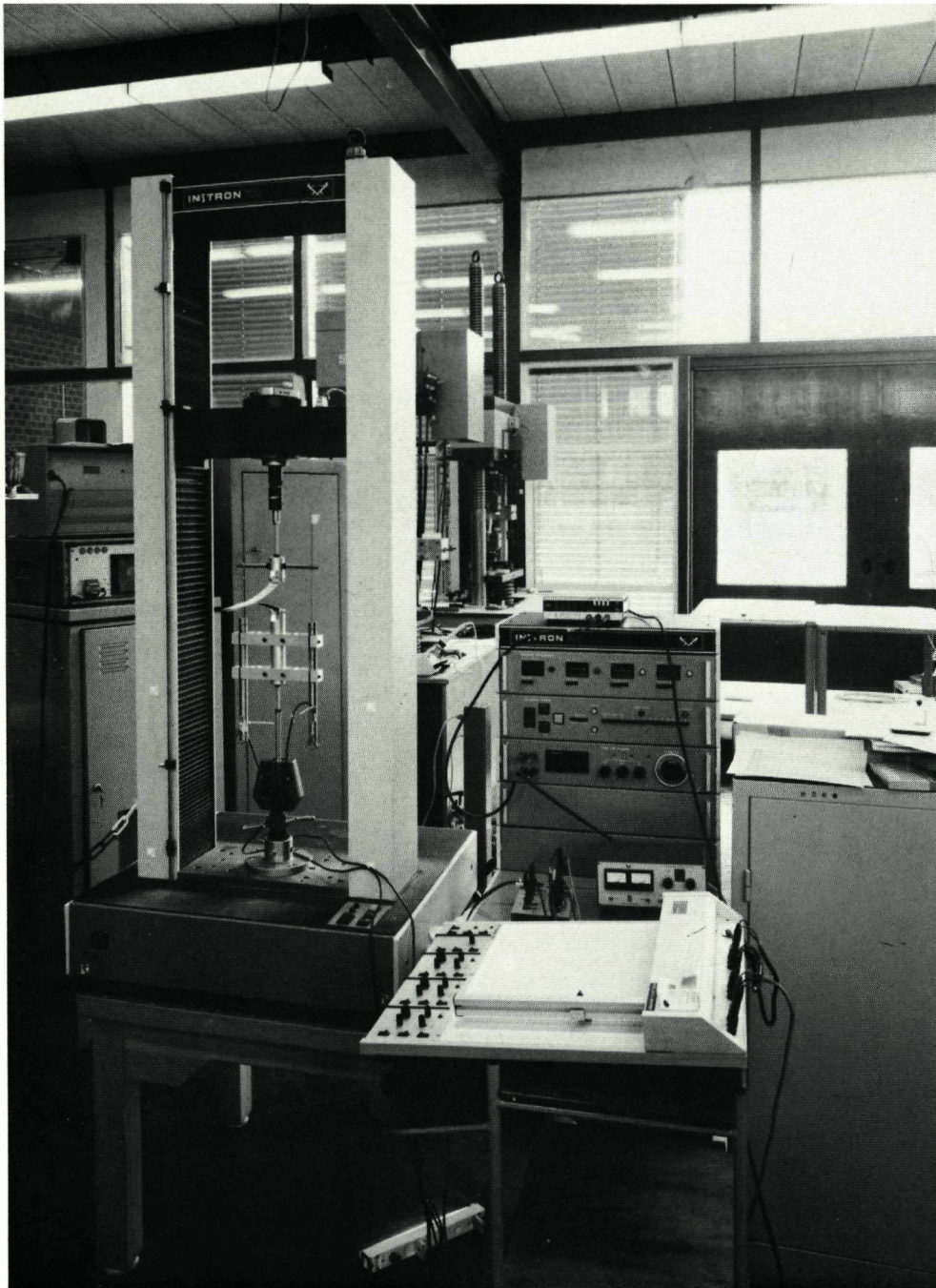
*Double Cantilever Beam specimen*



*End Notch Flexure specimen*

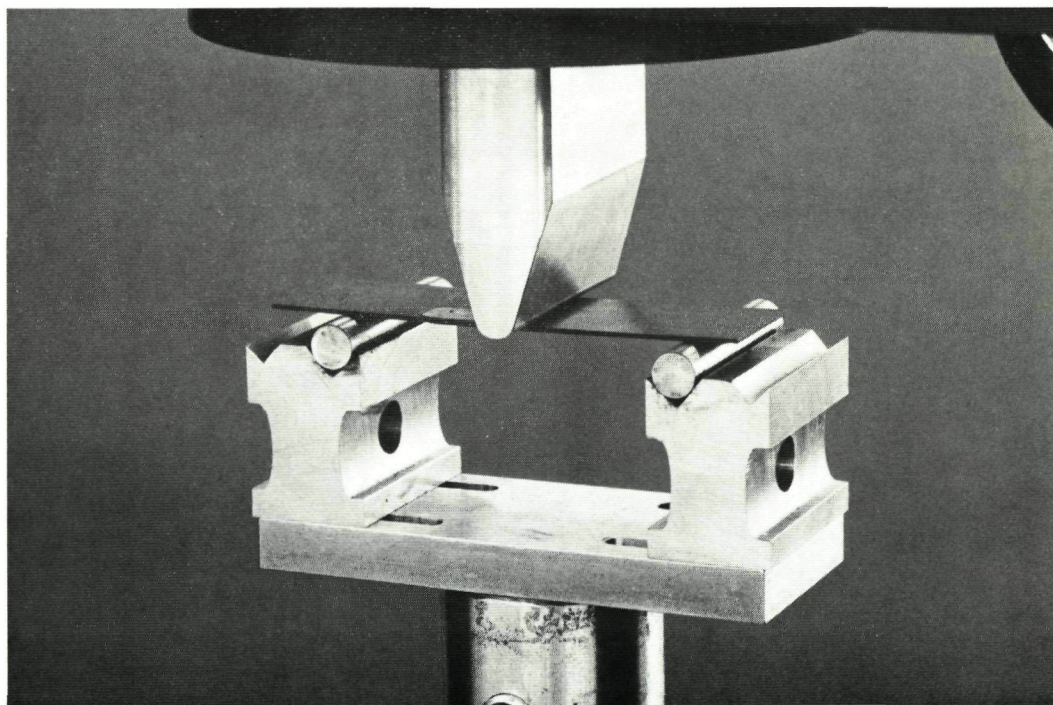
B146-08N

*Fig. 8 Double Cantilever Beam and End Notch Flexure specimens*



B146-07N

*Fig. 9 Arrangement for fracture toughness testing*



B146-08N

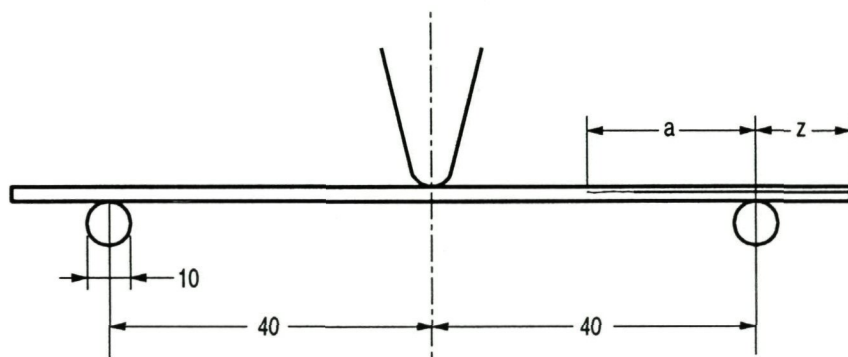
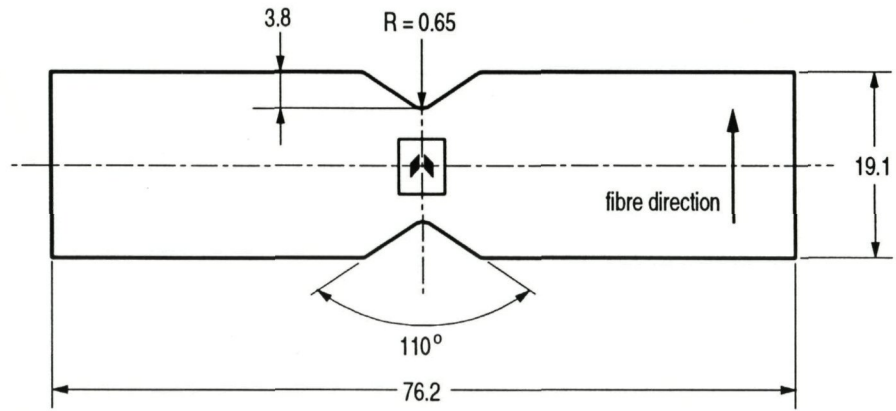
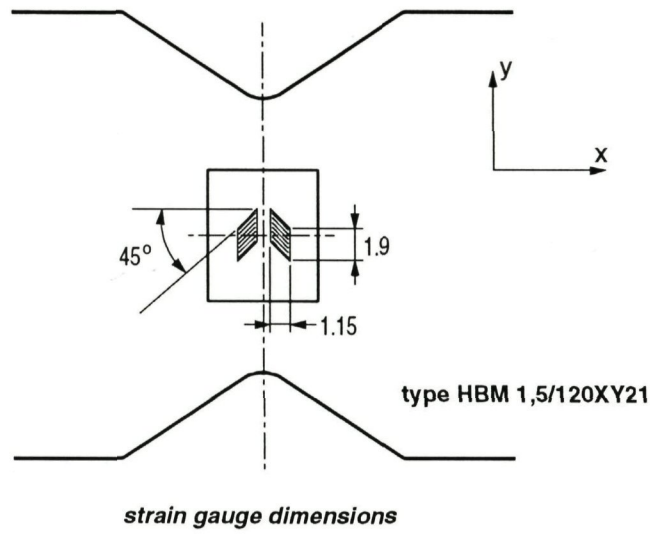


Fig. 10 3-point bending fixture used for mode II fracture energy testing.



*specimen dimensions*

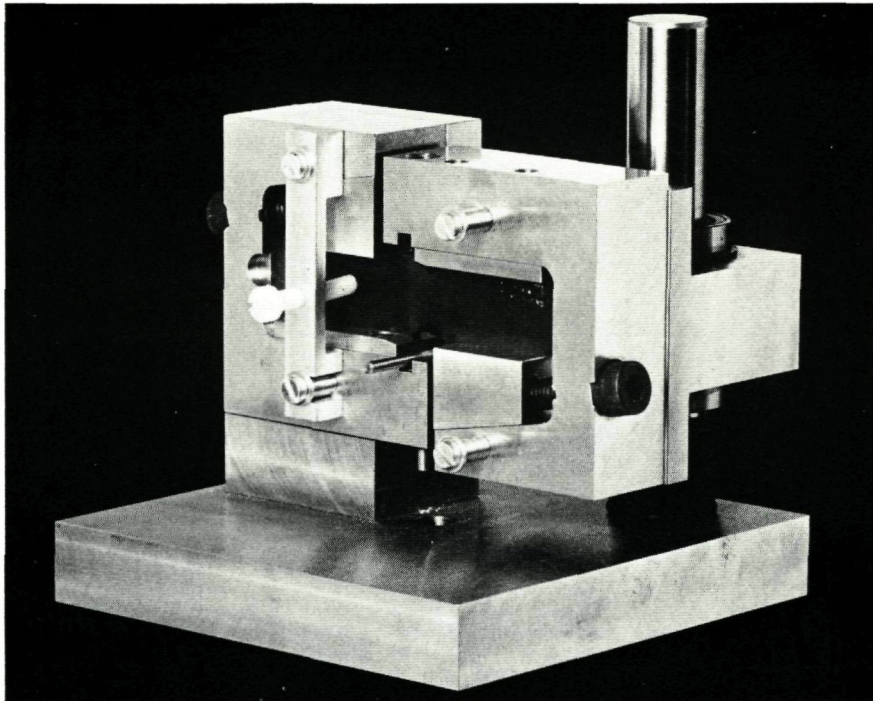
dimensions in mm



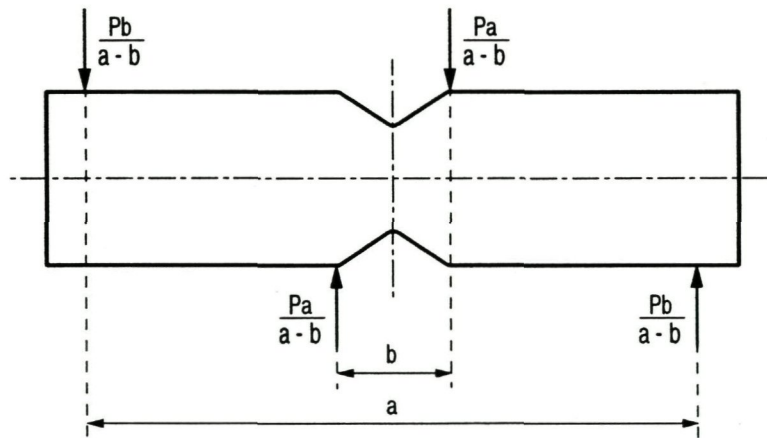
*strain gauge dimensions*

B146-08N

*Fig. 11 Iosupescu shear test specimen*



*Iosupescu test fixture*



B146-10N

*Fig. 12 Schematic force diagram for shear test specimen resulting from external load (P) on fixture*

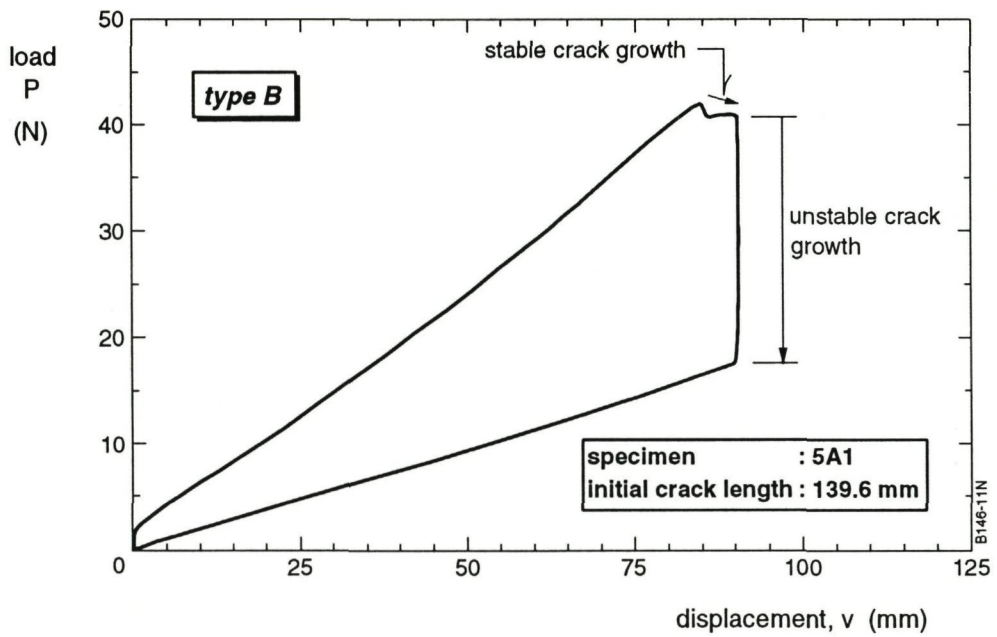
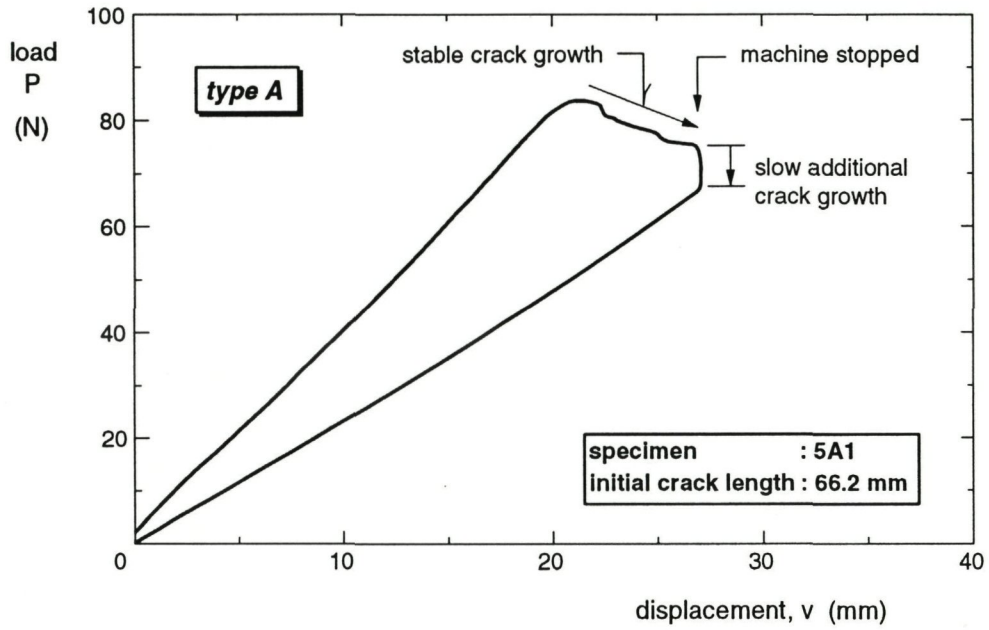


Fig. 13 Typical load-displacement curves measured during mode I fracture energy testing

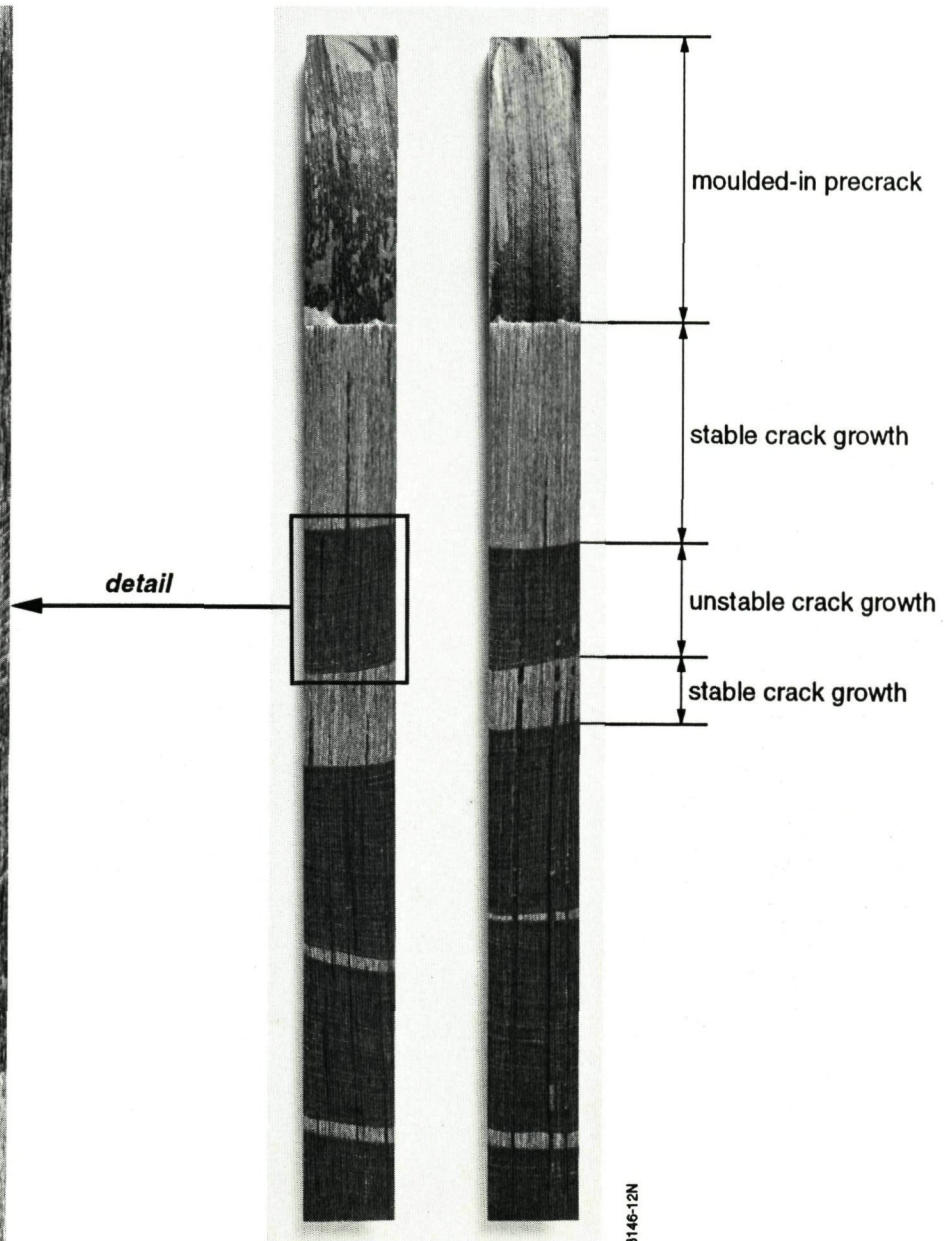


Fig. 14 Fracture surfaces of a DCB specimen



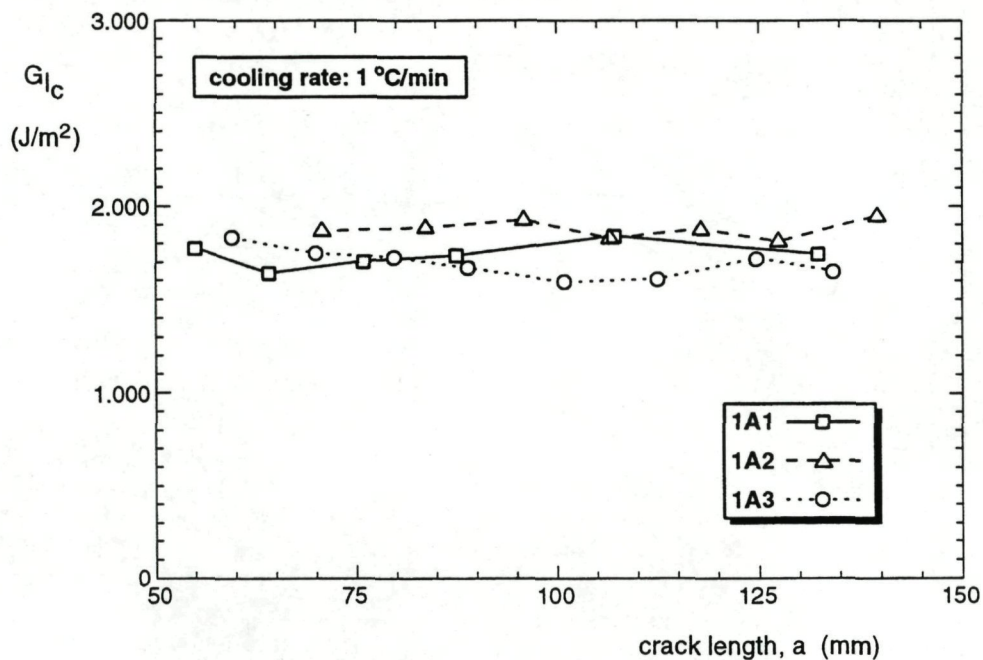


Fig. 15 Mode I fracture energy for cooling rate 1 °C/min

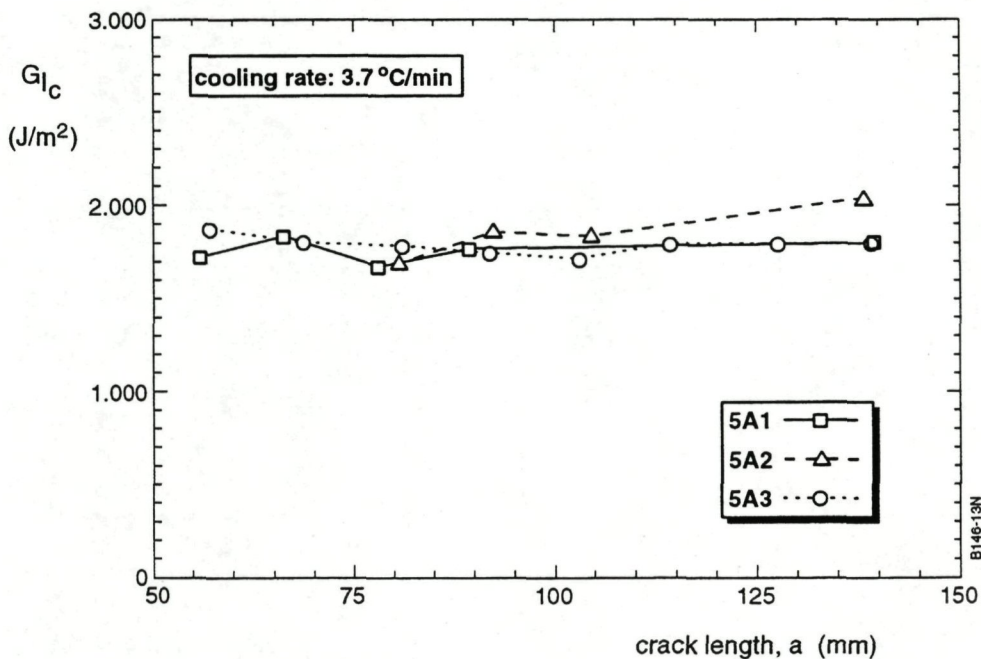


Fig. 16 Mode I fracture energy for cooling rate 3.7 °C/min

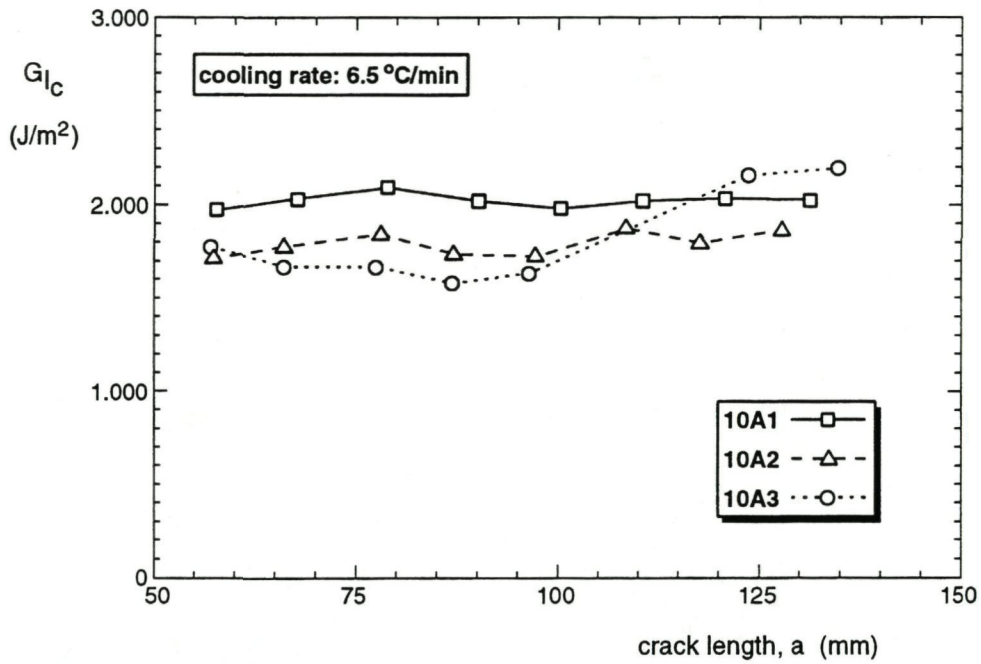


Fig. 17 Mode I fracture energy for cooling rate 6.5 °C/min

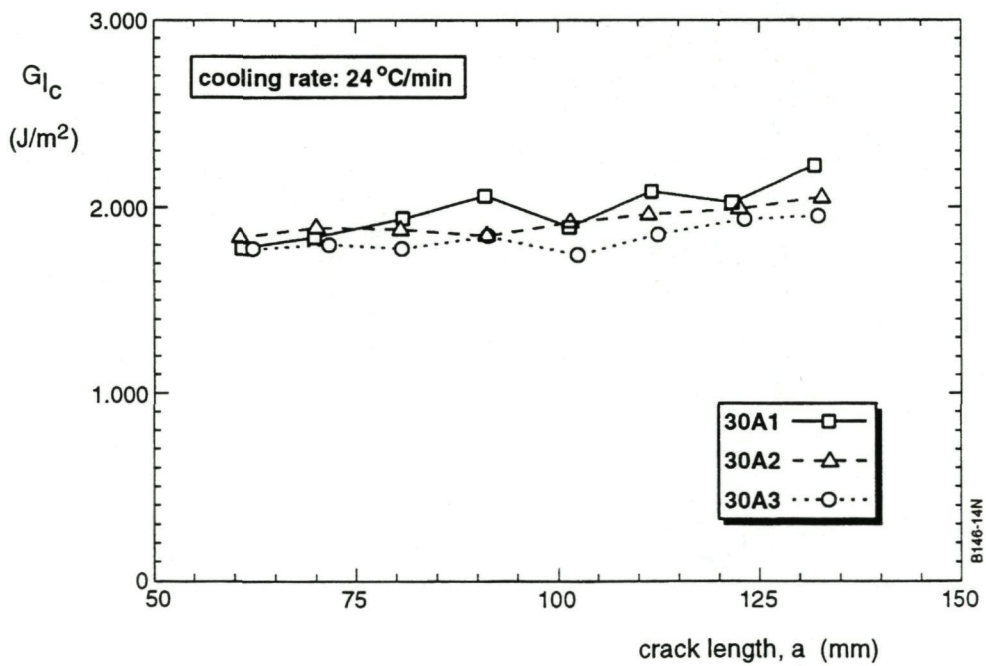


Fig. 18 Mode I fracture energy for cooling rate 24 °C/min

B146-14N

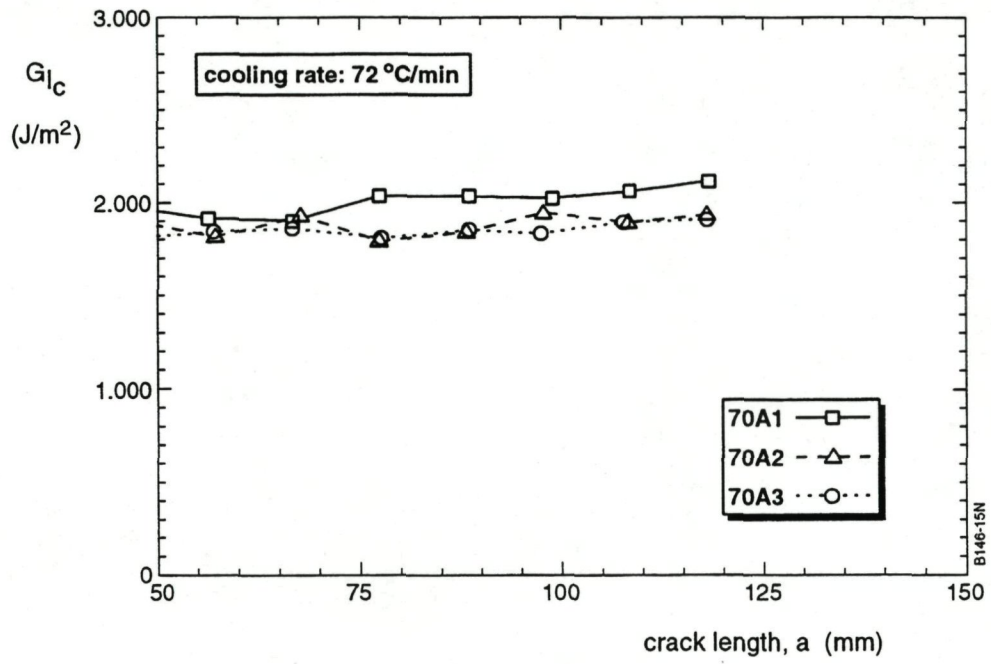


Fig. 19 Mode I fracture energy for cooling rate 72 °C/min

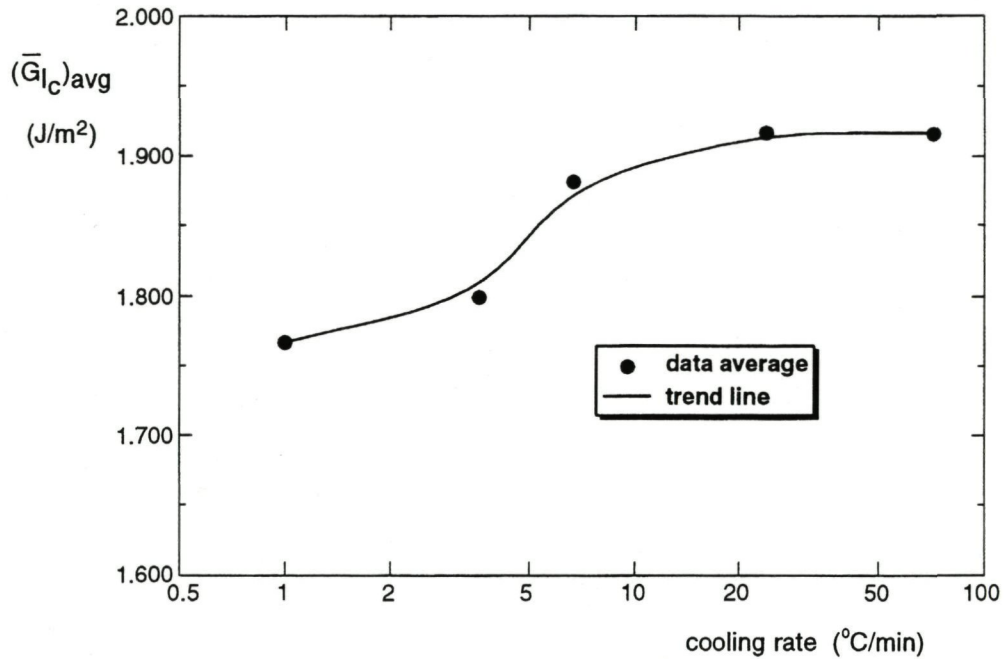


Fig. 20 Average mode I fracture energy versus cooling rate

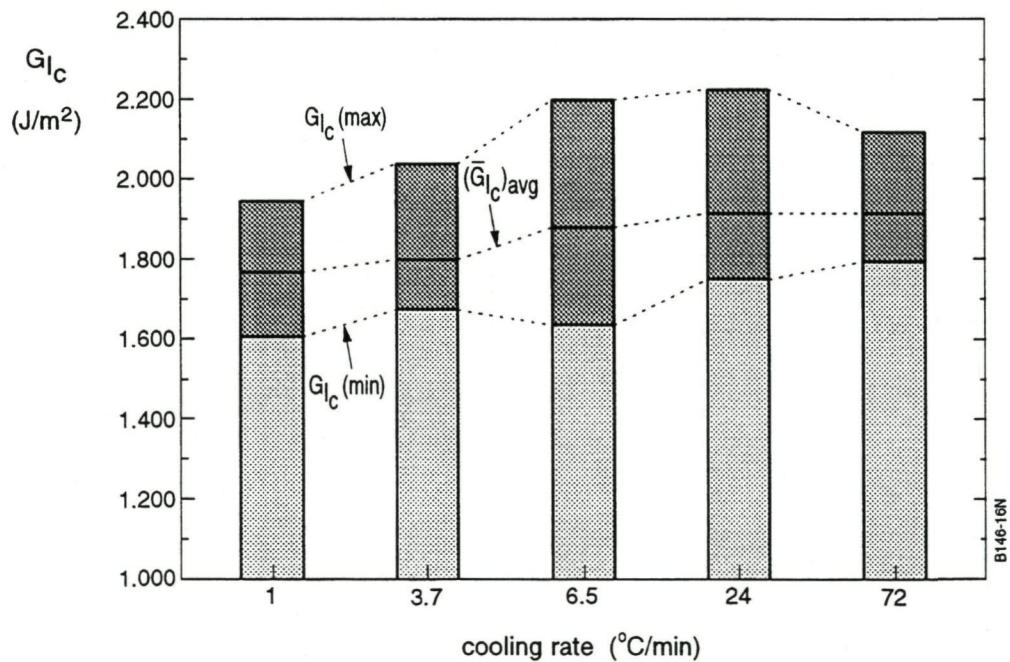


Fig. 21 Scatter in mode I fracture energy data. The minimum, average and maximum values measured for each cooling rate are indicated

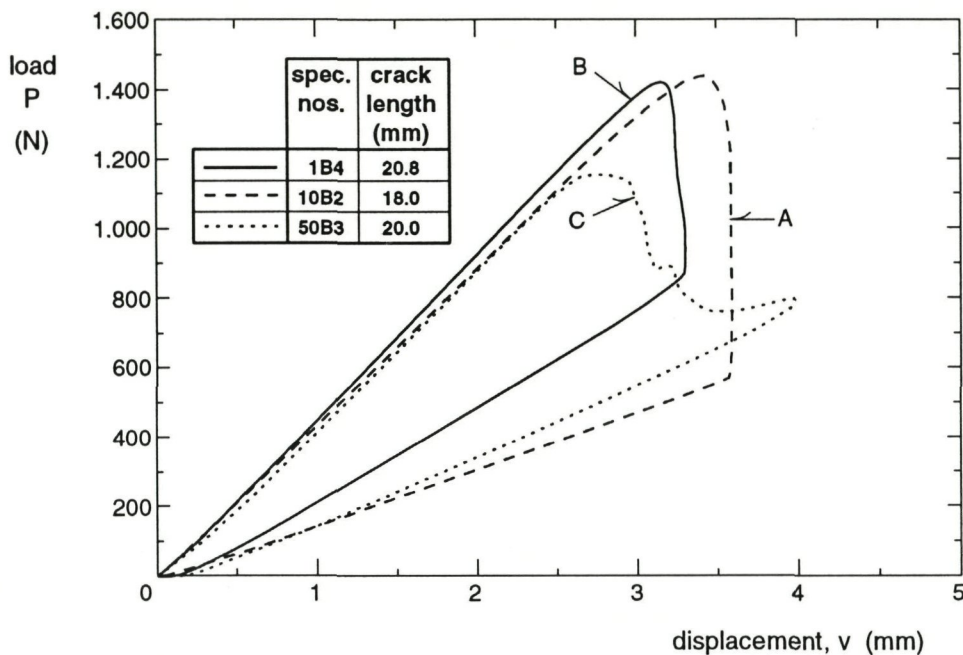


Fig. 22 Typical load - displacement traces recorded during tests on End Notch Flexure specimens

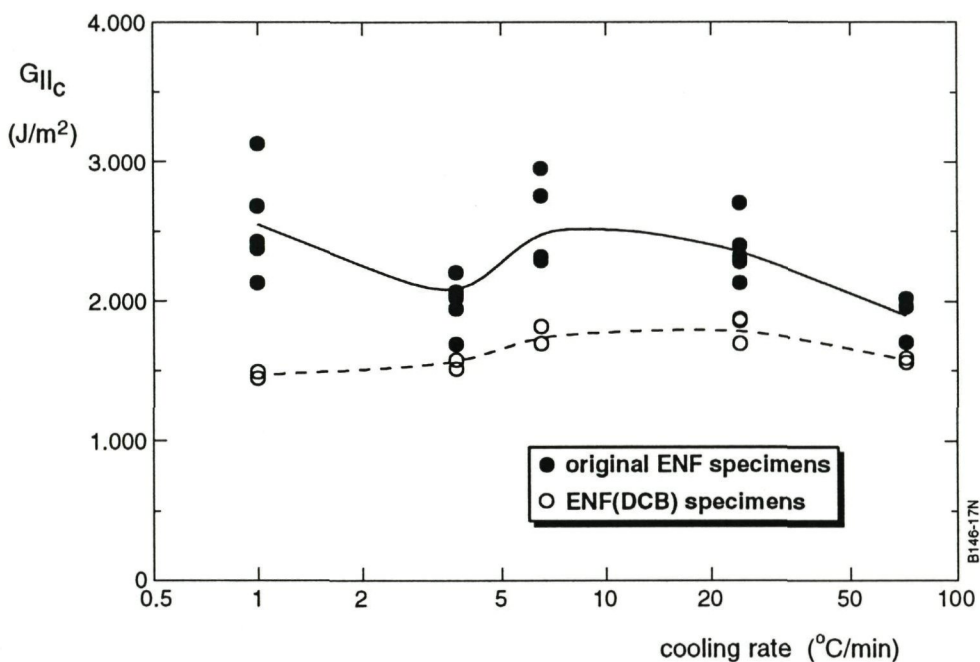


Fig. 23 Mode II fracture energy versus cooling rate. ENF(DCB) specimens were machined from previously test DCB specimens

B146-17N

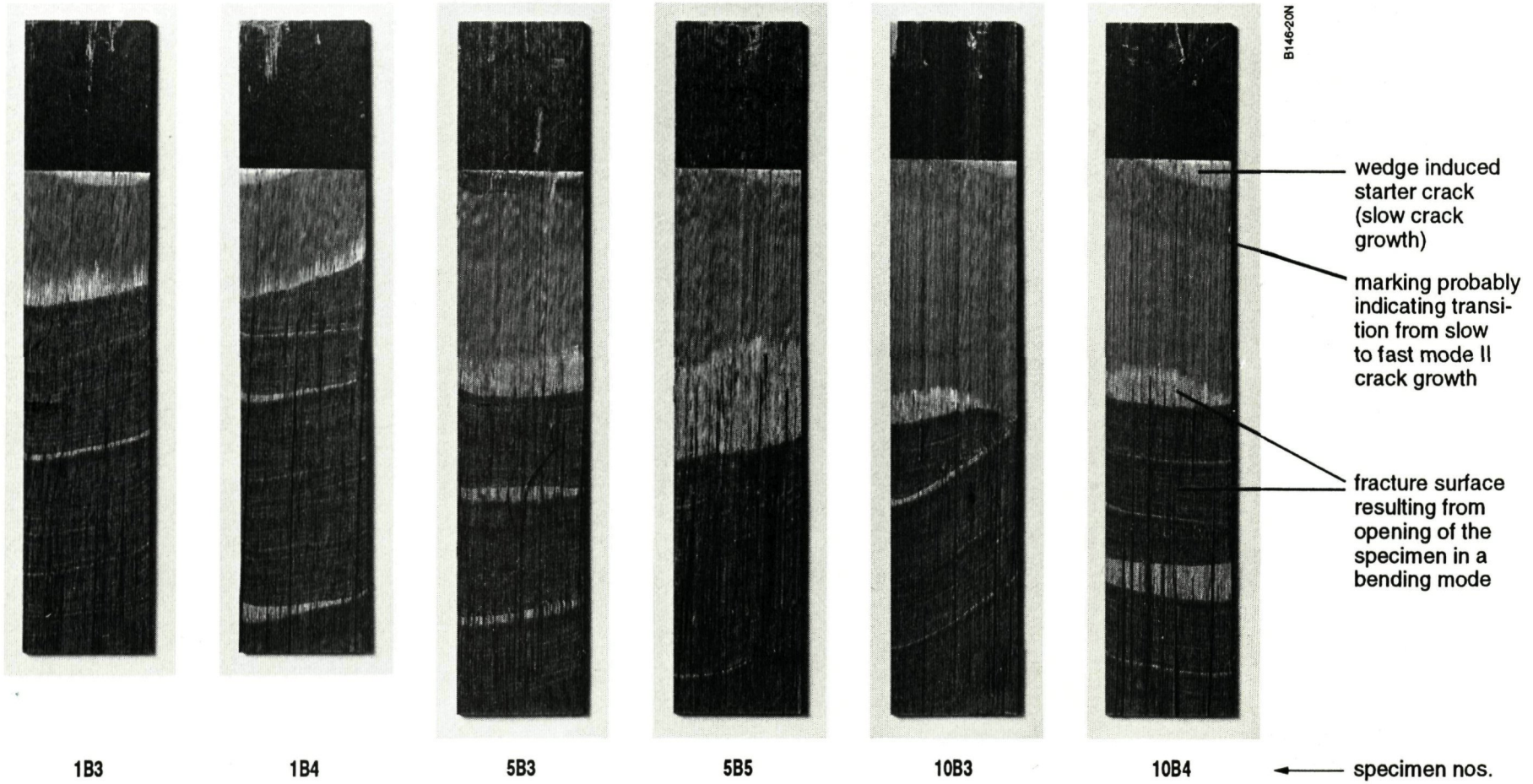


Fig. 24 Typical fracture surfaces of ENF specimens (cooling rates 1, 5 and 10°C/min)

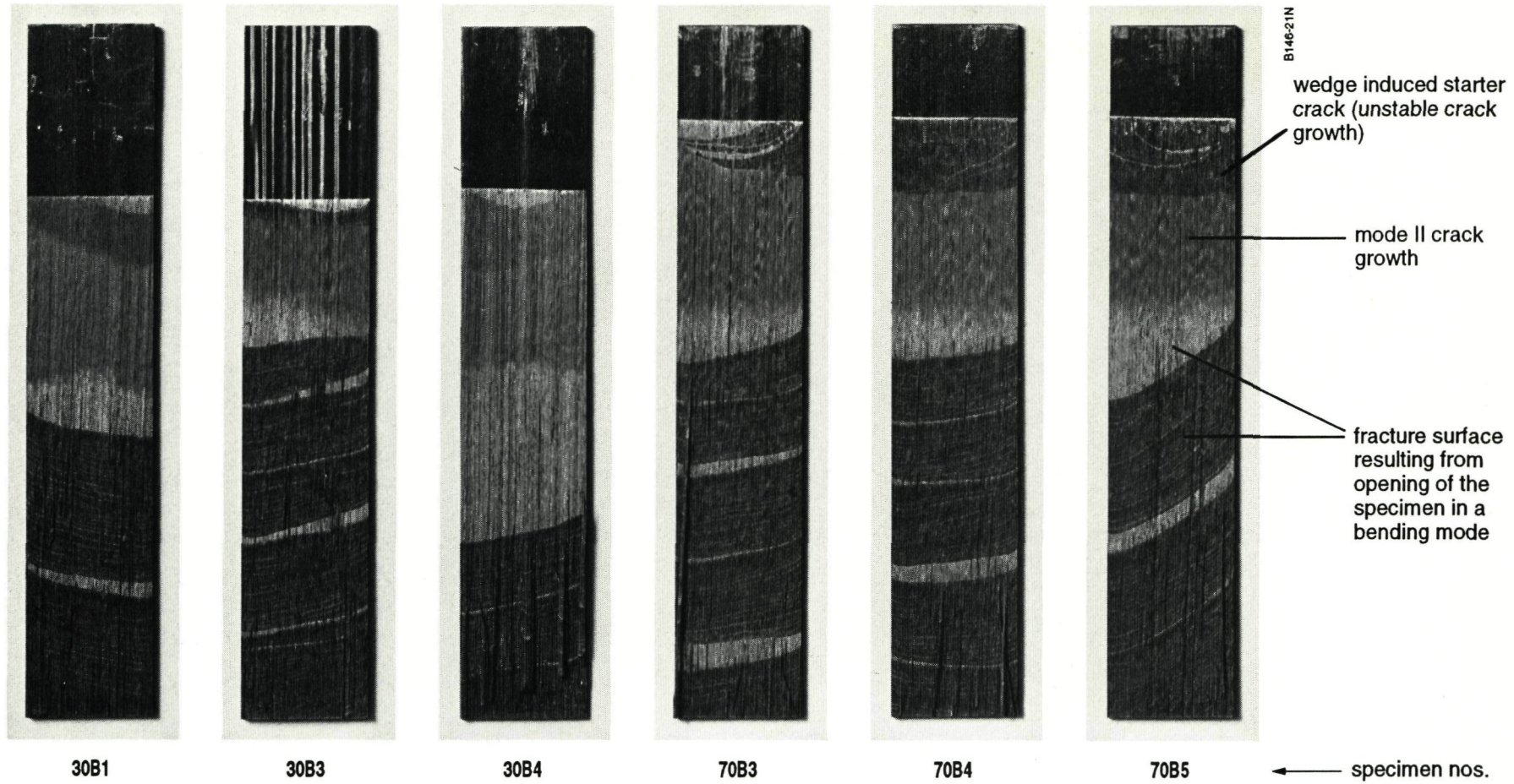


Fig. 25 Typical fracture surfaces of ENF specimens (cooling rates 30 and 70°C/min)

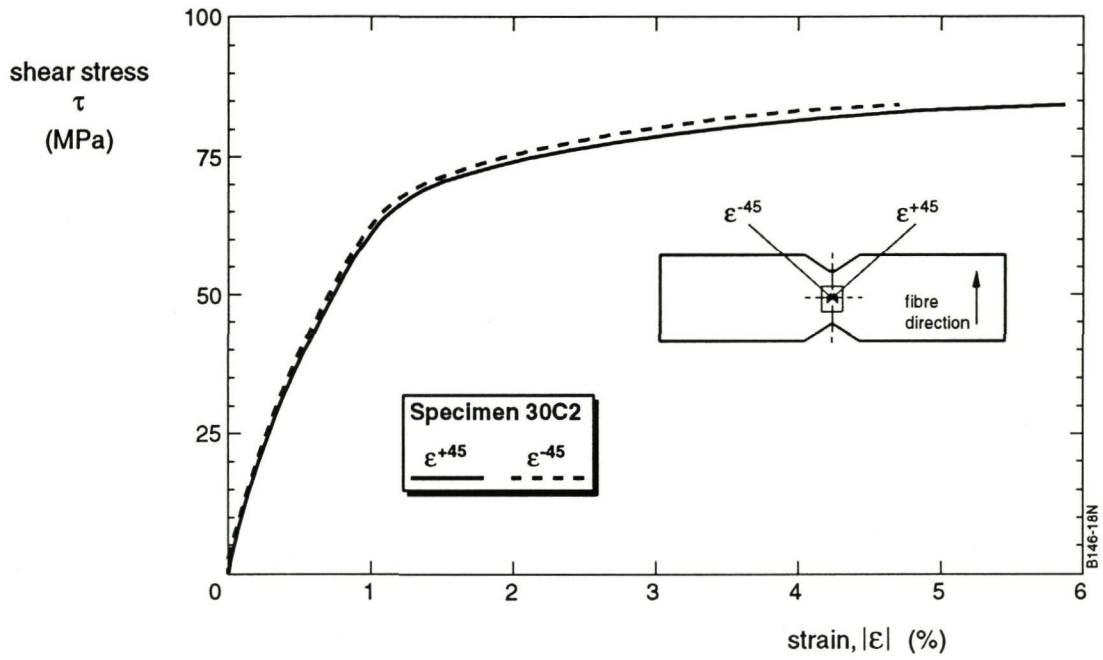


Fig. 26 Shear stress versus strain measured during test on specimen 30C2



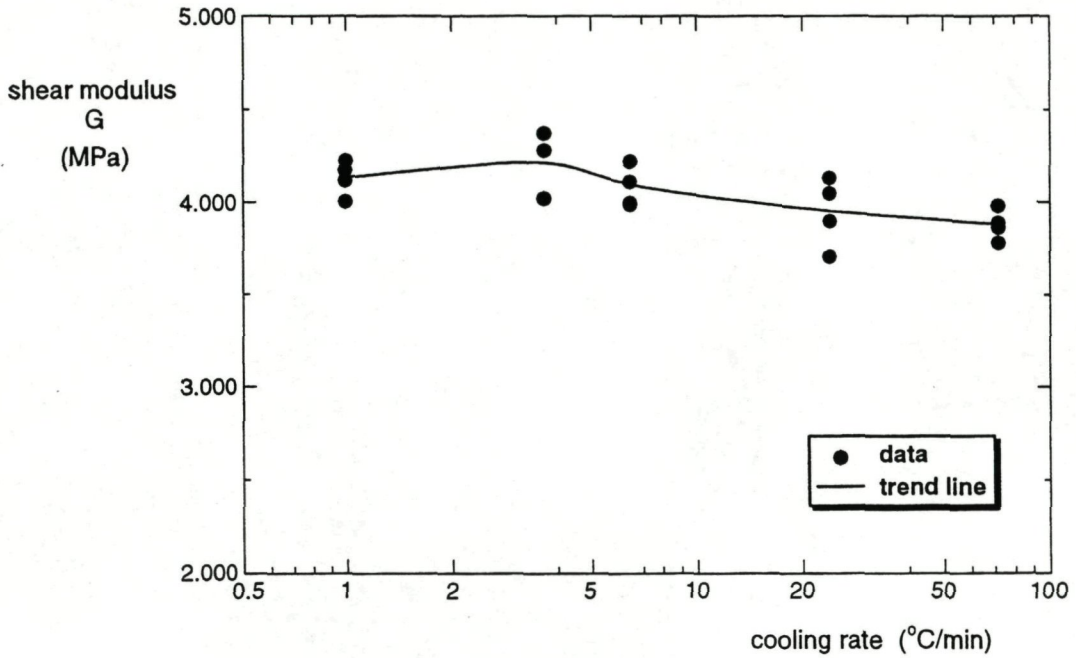


Fig. 27 Shear modulus versus cooling rate.  $G$  was calculated from the average slope of the measured stress-strain curves between 10 and 25 MPa

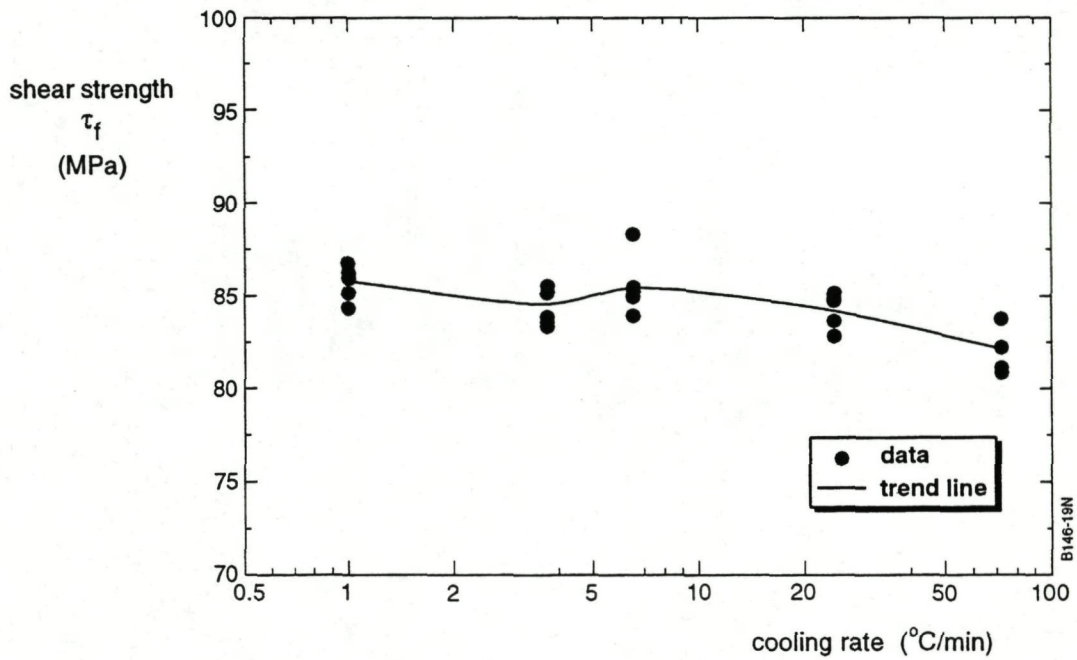


Fig. 28 Shear strength versus cooling rate.

B146-18N

